The PNJL model at imaginary chemical potential

Das PNJL-Modell bei imaginärem chemischen Potential

Master-Thesis von David Scheffler (korrigierte Version)

April 2010

TECHNISCHE UNIVERSITÄT DARMSTADT

Fachbereich Physik
Institut für Kernphysik
Nuclei, Hadrons & Quarks

The PNJL model at imaginary chemical potential
Das PNJL-Modell bei imaginärem chemischen Potential

vorgelegte Master-Thesis von David Scheffler (korrigierte Version)

1. Gutachten: Prof. Dr. J. Wambach
2. Gutachten: PD Dr. M. Buballa

Tag der Einreichung:

Abstract

In the Polyakov loop extended Nambu–Jona-Lasinio (PNJL) model, an effective model of QCD, the phase structure in the $\mu^2 - T$-plane is investigated. Due to the sign problem of lattice QCD, simulations on the lattice are not possible at $\mu^2 > 0$. As a workaround an extrapolation from imaginary to real chemical potential can be applied. Since direct calculations are possible in the PNJL model in both regions, we will use the PNJL model to check the reliability of this extrapolation method. We first study the PNJL model at imaginary quark chemical potential and find the Roberge-Weiss (RW) periodicity as well as the RW phase transition. In the imaginary chemical potential region the PNJL model possesses the extended $\mathbb{Z}_3$ symmetry of QCD. Using a PNJL model with two light and one heavier quark flavor we perform extrapolations from imaginary to real chemical potential and compare to direct calculations. In a two-flavor PNJL model we furthermore study the order of the RW phase transition endpoint for different Polyakov loop potentials and analyze its dependence on the relative strength of the potentials. Implications for the phase diagram are discussed.

Zusammenfassung

In dem um den Polyakov-Loop erweiterten Nambu–Jona-Lasinio (PNJL) Modell, einem effektiven Modell der QCD, wird das Phasendiagramm in der $\mu^2 - T$-Ebene untersucht. Wegen des Vorzeichenproblems der Gitter-QCD sind keine Simulationen für $\mu^2 > 0$ auf dem Gitter möglich. Um das Problem zu umgehen, kann von Ergebnissen bei imaginärem chemischen Potential zu reellem chemischen Potential extrapoliert werden. Da im PNJL Modell direkte Rechnungen in beiden Bereichen möglich sind, nutzen wir es um die Zuverlässigkeit der Extrapolationsmethode zu untersuchen. Dazu erweitern wir zunächst das PNJL-Modell zu imaginärem chemischen Potential und finden sowohl die Periodizität nach Roberge-Weiss (RW) als auch den RW-Phasenübergang. Im Bereich von imaginärem chemischen Potential besitzt das PNJL-Modell die erweiterte $\mathbb{Z}_3$ Symmetrie der QCD. In einem PNJL Modell mit zwei leichten und einem schwereren Quarkflavor führen wir Extrapolationen von imaginärem zu reellem chemischen Potential durch und vergleichen mit direkten Rechnungen. Außerdem bestimmen wir in einem PNJL Modell mit zwei Quarkflavors die Ordnung des Endpunkts des RW-Phasenübergangs bei verschiedenen Polyakov-Loop Potentialen und untersuchen die Abhängigkeit von der relativen Stärke der Potentiale. Mögliche Auswirkungen auf das Phasendiagramm werden diskutiert.

Contents

1 Introduction

Quantum chromodynamics (QCD) is a fascinating subject of theoretical physics. It incorporates the peculiar features of asymptotic freedom and confinement, the latter being yet unexplained. QCD provides a rich phase diagram with phases ranging from quarks bound to hadrons at low temperature and chemical potential to the quark gluon plasma (QGP) in the high temperature and density region, where the constituents are deconfined [1]. Color superconducting phases are expected at high densities [2].

In the last years lattice QCD as an ab initio approach has made huge progress in describing the thermodynamics of QCD and has provided important contributions to the understanding of the QCD phase diagram [3, 4]. The rapid development of computer power and new techniques make it possible to use larger lattices and smaller quark masses. Small lattices and unphysically large quark masses have been shortcomings of the lattice simulations before.

However computer power is not the only limitation of the lattice approach. While it gives valuable results for zero quark chemical potential ($\mu = 0$), it has a conceptual problem when calculating at $\mu \neq 0$. For finite real chemical potential the fermion determinant, which is used as a probability weight in the Monte Carlo sampling, becomes complex and thus the method fails. This is known as the "sign problem" [5].

1.1 Lattice QCD simulations at finite density

There are several methods proposed to circumvent this problem. For a review of lattice QCD at finite density see [6] and contributions to [3].

The first method is to use a Taylor series expansion performed at $\mu = 0$. That means to calculate derivatives of the thermodynamic potential with respect to μ/T, where T is the temperature, at $\mu = 0$ and with that Taylor series then extrapolate to $\mu/T > 0$. This is in principle possible and has already been done on the lattice for small values of μ/T (e.g. in [7]), though the radius of convergence is still unclear.

The second method is quite similar. Since the sign problem does not affect purely imaginary chemical potential, lattice simulations can easily be performed in that region. Again, an extrapolation to real μ can be done (e.g. see [8, 9, 10]). If one considers the $\mu^2 - T$ plane, this is an analytic continuation from negative to positive μ^2. This method is limited to a maximal imaginary part of the chemical potential of $\mu_I = \pi T/3$ where the first non-analyticity occurs in the imaginary chemical potential region. The applicability of the analytic continuation has been investigated in sign problem-free theories on the lattice [11]. Alternatively the grand canonical partition function in the imaginary chemical potential region $Z(V, T, i\mu)$ can be related to the canonical partition function $Z(V, T, n)$ at fixed quark number n via a Fourier transform [12].

A further method is the multi-parameter reweighting method [13].

1.2 The PNJL model as an effective model of QCD

Complementary to the lattice QCD approach, QCD can be investigated using effective models which are designed to have similar symmetries and effects as QCD. The Nambu–Jona-Lasinio (NJL) model [14, 15] already incorporates chiral symmetry breaking but not confinement. For reviews see [16, 17, 18]. For that reason the NJL model has been extended to include the Polyakov loop [19], which acts as an approximate order parameter for the deconfinement phase transition. The extended model is labeled "PNJL model".

Aside from lower computational needs, another advantage over the lattice simulation approach is that calculations at finite density are easily feasible. Because of that the (P)NJL model can been used to cross check the extrapolation techniques used in lattice QCD: A Taylor expansion of the pressure at $\mu = 0$ has been performed in a simple NJL model [20] and in a PNJL model [21]. Qualitative results have been confirmed in the Polyakov Quark Meson (PQM) model [22].

The extrapolation from imaginary chemical potential is a major topic of this thesis project. The PNJL model with two light quark flavors at imaginary chemical potential has already been investigated by Sakai et al. [23, 24, 25, 26, 27]. In this work we will also consider the strange quark, so we extend this approach to two light and one heavy quark flavors, which gives a more realistic description of QCD.

1.3 Phase structure at imaginary quark chemical potential

At imaginary quark chemical potential QCD has special properties. An extension of the $\mathbb{Z}_3$ symmetry of pure gauge theory leads to a periodicity with respect to the imaginary chemical potential [12]. One finds that the PNJL model likewise possesses the extended $\mathbb{Z}_3$ symmetry and hence has the RW periodicity [27]. In agreement with QCD a first order phase transition, the RW phase transition, occurs at high temperatures. At low temperatures the transition is continuous. The first order transition either ends in a second order endpoint or in a first order branching point. Recent lattice results [28, 29] indicate, that the point is of first order for very low and very high quark masses, and of second order for intermediate quark masses. An analysis in the two-flavor PNJL model yields a second order phase transition [27]. A first order point would have implications on the phase structure since then first order lines are expected to depart from it. This is then called a triple point as three phases coexist in that point.

We want to investigate the RW endpoint[1] in the PNJL model in more detail. Of special interest is the dependence of the order of that point on the quark mass and other model parameters. If it is a triple point, we will examine the attached first order lines.

1.4 Structure of this document

The content of this thesis is organized as follows: In the next chapter we will introduce essential properties of the PNJL model. Chapter 3 contains a discussion of the PNJL model at imaginary chemical potential. We will use the PNJL model in Chapter 4 to do extrapolations of (pseudo)

[1] We are aware that the first order line does not end there if it is a triple point. Nevertheless we will call it RW endpoint as the RW transition along fixed $\theta = (2k+1)\pi/3$ (where k is integer and $\theta = -i\mu/T$) ends there.

phase transition lines. A study of the order of the Roberge-Weiss transition endpoint will be presented in the subsequent Chapter 5. In the final chapter we will summarize our findings and give an outlook on remaining challenges.

Parts of this thesis had been prepared for the master project proposal [30].

2 The PNJL model

The discussion of the PNJL model with 2+1 flavors at real chemical potential will mainly follow [31].

2.1 Model setup

We consider two degenerate light quark flavors, up and down quarks, and additionally a heaver flavor, the strange quark. Quarks are the only dynamical degrees of freedom in the PNJL model. The scalar interaction channel in form of a four-quark pointlike interaction and the six-quark 't Hooft interaction are included.

$$\begin{aligned}\mathscr{L}_{\text{PNJL}} &= \bar{\psi}\left(i\gamma_\mu D^\mu - \hat{m}_f\right)\psi \\ &+ \frac{g_S}{2}\left[(\bar{\psi}\tau_a\psi)^2 + (\bar{\psi}i\gamma_5\tau_a\psi)^2\right] \\ &+ g_D\left[\det{}_f\left(\bar{\psi}(1-\gamma_5)\psi\right) + \det{}_f\left(\bar{\psi}(1+\gamma_5)\psi\right)\right] \\ &+ \mathscr{U}_{\text{Polyakov}}(\Phi[A], \bar{\Phi}[A], T)\end{aligned} \tag{2.1}$$

ψ is the three-flavor quark spinor, $\hat{m}_f$ denotes a diagonal matrix containing the bare quark masses, g_S and g_D are coupling constants. We also have the covariant derivative $D^\nu = \partial^\nu + iA^\nu - i\mu\delta^\nu_0$ along with the gauge fields $A^\nu = \delta^\nu_0 g A^0_a \frac{\lambda^a}{2}$ and the quark chemical potential μ. Furthermore we use the Gell-Mann matrices λ_a (τ_a) in color (flavor) space (with $\tau_0 = \sqrt{2/3}\mathbb{1}$).

Φ and $\bar{\Phi}$ are the traced Polyakov loop and its conjugate introduced in the following subsection. The Polyakov loop potential $\mathscr{U}_{\text{Polyakov}}(\Phi[A], \bar{\Phi}[A], T)$ is the effective potential for the gluonic part of the theory. Possible parameterizations will be given in a later section.

2.1.1 Symmetries

In the chiral limit ($m_f = 0$) the Lagrangian density has an exact $SU(3)_L \times SU(3)_R \times U(1)_V \times SU(3)_c$ symmetry.

Finite quark masses explicitly break chiral symmetry. Since we will use equal masses for up and down quarks isospin symmetry will remain intact. We will find that chiral symmetry is additionally broken spontaneously through dynamical mass generation (even in the chiral limit). The 't Hooft-term explicitly breaks the axial $U(1)$ symmetry.

The chiral quark condensates $\sigma_{ud} \equiv \sigma_u = \langle\bar{u}u\rangle = \langle\bar{d}d\rangle = \sigma_d$ and $\sigma_s = \langle\bar{s}s\rangle$ are exact order parameters for the chiral symmetry in the chiral limit where the bare quark masses are set to zero. With finite bare quark masses the light quark chiral condensate still serves as an approximate order parameter for the chiral phase transition.

The Polyakov loop is a Wilson loop closed around the periodic Euclidean time direction. It is defined as a matrix in color space

$$L(\vec{x}) = \mathscr{P} \exp\left[i \int_0^{1/T} d\tau \, A_4(\vec{x}, \tau) \right] \tag{2.2}$$

with $A_4 = iA_0$ and $\mathscr{P}$ denotes the path ordering of the exponential. In the Polyakov gauge the matrix can be given in diagonal form by

$$L = \exp\left[i(\phi_3 \lambda_3 + \phi_8 \lambda_8) \right]. \tag{2.3}$$

Its traced expectation values are given by

$$\Phi = \frac{1}{N_c} \left\langle \operatorname{tr} L \right\rangle, \qquad \bar{\Phi} = \frac{1}{N_c} \left\langle \operatorname{tr} L^\dagger \right\rangle \tag{2.4}$$

where the number of colors $N_c = 3$ is the physical one.

In the pure gauge case (which is realized in the infinite quark mass limit) the Polyakov loop expectation value Φ is an exact order parameter of the $\mathbb{Z}_3$ symmetry which is spontaneously broken at high temperatures. The $\mathbb{Z}_3$ symmetry appears as the center symmetry of the $SU(3)_c$ gauge symmetry. According to lattice QCD, in the pure gauge case the deconfinement phase transition along the temperature axis occurs at $T_c = 270$ MeV and is of first order for $N_c = 3$.

In QCD the Polyakov loop expectation values measure the free energy of a static quark F_q and antiquark $F_{\bar{q}}$ [32]

$$\Phi = \exp\left(-\frac{F_q}{T} \right), \qquad \bar{\Phi} = \exp\left(-\frac{F_{\bar{q}}}{T} \right). \tag{2.5}$$

In the confined phase it is not possible to create a single quark ($F_q = \infty$), therefore $\Phi = 0$, whereas in the deconfined phase the free energy is finite and Φ is non-zero.

However, in the presence of dynamical quarks the $\mathbb{Z}_3$ symmetry is not exact any more. Still Φ is considered to be an approximate order parameter of the deconfinement phase transition. An in-depth analysis of the center symmetry can be found in [32].

Summarizing the behavior of QCD we can state that in the low temperature and low density region, quarks are confined to hadrons and the chiral symmetry is broken by the dynamically generated finite quark masses. In terms of the order parameters this means that $\sigma_f \neq 0$ and $\Phi \approx 0$. When the temperature and density increase quarks become free (deconfined) and the chiral symmetry is restored ($\sigma_f \approx 0$ and $\Phi \approx 1$). Quarks and gluons then form a quark gluon plasma.

In the PNJL model the order parameters show the same behavior though no hadrons and gluons are included as degrees of freedom. Still, confinement is not correctly reproduced since e. g. mesons can decay into quarks [33].

2.1.2 Mean field approximation

In mean field approximation we expand the quark fields around their expectation values and neglect higher order fluctuations. Exemplarily, we obtain

$$(\bar{u}u)^2 = \left(\langle \bar{u}u \rangle + \delta(\bar{u}u) \right)^2 \approx \langle \bar{u}u \rangle^2 + 2 \langle \bar{u}u \rangle \delta(\bar{u}u) = 2 \langle \bar{u}u \rangle \bar{u}u - \langle \bar{u}u \rangle^2. \tag{2.6}$$

The expectation values Φ and $\bar{\Phi}$ from Eq. (2.4) are assumed to be real and independent [31]. The actual dependence on ϕ_3 and ϕ_8 is ignored, instead Φ and $\bar{\Phi}$ will be used as model variables. This is treated differently in [21] where $\phi_3, \phi_8 \in \mathbb{R}$ are used to parameterize the Polyakov loop. From equations (2.3) and (2.4) we see that this would imply that Φ and $\bar{\Phi}$ are connected by complex conjugation. However, this either means that $\Phi = \bar{\Phi}$ or that these quantities take complex values which is in conflict with the notion that the Polyakov loop expectation values are connected to the free energy of a static quark or antiquark, see (2.5) above.

We can write the mean field Langrangian as

$$\begin{aligned}\mathcal{L}_{\text{MFA}} = &\bar{\psi}\left(i\gamma_\mu D^\mu - \hat{M}_f\right)\psi \\ &+ g_S\left(\sigma_u^2 + \sigma_d^2 + \sigma_s^2\right) + 4g_D\sigma_u\sigma_d\sigma_s \\ &+ \mathcal{U}_{\text{Polyakov}}(\Phi, \bar{\Phi}, T)\end{aligned} \tag{2.7}$$

with effective masses

$$\left.\begin{aligned}M_u &= m_u - 2g_S\sigma_u - 2g_D\sigma_d\sigma_s \\ M_d &= m_d - 2g_S\sigma_d - 2g_D\sigma_u\sigma_s\end{aligned}\right\} \Rightarrow M_{ud} = m_{ud} - 2\sigma_{ud}\left(g_S + g_D\sigma_s\right) \tag{2.8}$$
$$M_s = m_s - 2g_S\sigma_s - 2g_D\sigma_u\sigma_d \quad \Rightarrow M_s = m_s - 2g_S\sigma_s - 2g_D{\sigma_{ud}}^2.$$

The Polyakov loop potential $\mathcal{U}_{\text{Polyakov}}$ which will also contribute to the total energy will be discussed in a later section.

2.1.3 Thermodynamic potential

The thermodynamic potential in the grand canonical formulation including temperature and finite density dependence is given as:

$$\begin{aligned}\Omega(T, \mu; \sigma_f, \Phi, \bar{\Phi}) = -2\sum_f \int \frac{d^3p}{(2\pi)^3}\Big\{&N_c E_f(p) \\ &+ T\log\left[1 + 3\Phi e^{-\frac{E_f-\mu}{T}} + 3\bar{\Phi}e^{-2\frac{E_f-\mu}{T}} + e^{-3\frac{E_f-\mu}{T}}\right] \\ &+ T\log\left[1 + 3\bar{\Phi} e^{-\frac{E_f+\mu}{T}} + 3\Phi e^{-2\frac{E_f+\mu}{T}} + e^{-3\frac{E_f+\mu}{T}}\right]\Big\} \\ &+ g_S({\sigma_u}^2 + {\sigma_d}^2 + {\sigma_s}^2) + 4g_D\sigma_u\sigma_d\sigma_s + \mathcal{U}_{\text{Polyakov}}.\end{aligned} \tag{2.9}$$

$E_f(p) = \sqrt{p^2 + {M_f}^2}$ denotes the single-quark energy with the absolute value of the 3-momentum $p = |\vec{p}|$.

The (P)NJL model is not renormalizable [16], and the integral of Equation (2.9) will diverge. Therefore we will need to regularize it. We will use two different versions. Variant I: We apply a sharp three-momentum cut-off only to the vacuum part of all momentum integrals (first summand in this case) since the medium parts are finite already. Variant II: The three-momentum cut-off is also applied to the medium parts of the integrals. Only variant I gives the correct (Stefan-Boltzmann) limit for high temperatures.

Gap equations and effective quark masses

From the stationary conditions,

$$\frac{\partial\Omega}{\partial\sigma_u}=0,\qquad \frac{\partial\Omega}{\partial\sigma_d}=0,\qquad \frac{\partial\Omega}{\partial\sigma_s}=0,\qquad \frac{\partial\Omega}{\partial\Phi}=0,\qquad \frac{\partial\Omega}{\partial\bar{\Phi}}=0, \tag{2.10}$$

we get the so-called gap equations which are solved numerically.

There can be several roots of the gap equations. They are inserted into the thermodynamic potential (2.9) and the one with lowest value is taken as the stable solution.

Special cases

Let us consider how the model behaves in some special cases.

As we see from Eq. (2.9) the Polyakov loop has no influence at $T=0$, where we recover the NJL model.

From the charge conjugation symmetry

$$\Omega(T,-\mu;\sigma_f,\bar{\Phi},\Phi)=\Omega(T,\mu;\sigma_f,\Phi,\bar{\Phi}) \tag{2.11}$$

we can conclude that Φ and $\bar{\Phi}$ must be equal at $\mu=0$.

In the fully deconfined limit ($\Phi=\bar{\Phi}\to 1$) the thermal part goes over into the familiar NJL expression:

$$\begin{aligned} &T\log\left[1+3\Phi e^{-\frac{E-\mu}{T}}+3\bar{\Phi}e^{-2\frac{E-\mu}{T}}+e^{-3\frac{E-\mu}{T}}\right]+T\log\left[1+3\bar{\Phi}e^{-\frac{E+\mu}{T}}+3\Phi e^{-2\frac{E+\mu}{T}}+e^{-3\frac{E+\mu}{T}}\right]\\ &\to N_c T\left(\log\left[1+e^{-\frac{E-\mu}{T}}\right]+\log\left[1+e^{-\frac{E+\mu}{T}}\right]\right) \qquad \text{for}\quad N_c=3 \end{aligned} \tag{2.12}$$

For $\Phi=\bar{\Phi}\to 0$, when the system is confined, we obtain

$$\begin{aligned} &T\log\left[1+3\Phi e^{-\frac{E-\mu}{T}}+3\bar{\Phi}e^{-2\frac{E-\mu}{T}}+e^{-3\frac{E-\mu}{T}}\right]+T\log\left[1+3\bar{\Phi}e^{-\frac{E+\mu}{T}}+3\Phi e^{-2\frac{E+\mu}{T}}+e^{-3\frac{E+\mu}{T}}\right]\\ &\to T\log\left[1+e^{-\frac{3E-\mu_B}{T}}\right]+T\log\left[1+e^{-\frac{3E+\mu_B}{T}}\right] \qquad \text{with}\quad \mu_B=3\mu \end{aligned} \tag{2.13}$$

and recognize that one- and two-quark contributions are suppressed.

2.1.4 Parameters

As we just discussed, the vacuum properties do not change from NJL to PNJL. Since all (NJL) parameters are fixed at at $T=\mu=0$ we can use a standard NJL model parameter set. For the first part of the current work we will take a parameter set from [18]. It is adjusted to reproduce the pion, kaon and eta prime masses as well as the pion decay constant f_π. Values are given in Table 2.1. Parameters for the Polyakov loop will be discussed in the next section.

2.2 Polyakov loop potentials

There are three popular parameterizations for the Polyakov loop potential $\mathcal{U}_{\text{Polyakov}}$. These potentials are designed to have the $\mathbb{Z}_3$ symmetry of pure gauge and to exhibit a first order deconfinement phase transition at $T_c=270$ MeV. All parameters are fixed at vanishing chemical potential and no dependence on the chemical potential is included.

Λ in MeV	m_{ud} in MeV	m_s in MeV	$g_S\Lambda^2$	$g_D\Lambda^5$
631.4	5.5	135.7	3.67	−9.29

Table 2.1: Parameter choice (NJL part), taken from [18]

The polynomial potential,

$$\begin{aligned}\frac{\mathcal{U}_{\text{poly}}}{T^4} &= -\frac{b_2(T)}{2}\Phi\bar{\Phi} - \frac{b_3}{6}(\Phi^3+\bar{\Phi}^3) + \frac{b_4}{4}(\Phi\bar{\Phi})^2 \\ \text{with} \quad b_2(T) &= a_0 + a_1\frac{T_0}{T} + a_2\left(\frac{T_0}{T}\right)^2 + a_3\left(\frac{T_0}{T}\right)^3,\end{aligned} \tag{2.14}$$

has been proposed in [34] with parameters $a_0 = 6.75$, $a_1 = -1.95$, $a_2 = 2.625$, $a_3 = -7.44$, $b_3 = 0.75$, $b_4 = 7.5$ and $T_0 = 270$ MeV.

A logarithmic parameterization $\mathcal{U}_{\log}$ was introduced in [21],

$$\begin{aligned}\frac{\mathcal{U}_{\log}}{T^4} &= -\frac{a(T)}{2}\Phi\bar{\Phi} + b(T)\log\left[1 - 6\Phi\bar{\Phi} + 4(\Phi^3+\bar{\Phi}^3) - 3(\Phi\bar{\Phi})^2\right] \\ \text{with} \quad a(T) &= a_0 + a_1\frac{T_0}{T} + a_2\left(\frac{T_0}{T}\right)^2 \quad \text{and} \quad b(T) = b_3\left(\frac{T_0}{T}\right)^3\end{aligned} \tag{2.15}$$

with parameters $a_0 = 3.51$, $a_1 = -2.47$, $a_2 = 15.2$, $b_3 = -1.75$ and $T_0 = 270$ MeV.

For fixing the parameters of abovementioned potentials the Stefan-Boltzmann limit is used as a constraint. Furthermore properties like the pressure at vanishing chemical potential are fit to lattice calculations.

The third parameterization, $\mathcal{U}_{\text{Fuku}}$, is inspired by a strong-coupling analysis [31],

$$\frac{\mathcal{U}_{\text{Fuku}}}{T^4} = -bT\left(54e^{-a/T}\Phi\bar{\Phi} + \log\left[1 - 6\Phi\bar{\Phi} + 4(\Phi^3+\bar{\Phi}^3) - 3(\Phi\bar{\Phi})^2\right]\right). \tag{2.16}$$

The parameters a and b control the transition temperature and the strength of the mixing between the chiral and deconfinement phase transitions respectively. For $N_f = 2{+}1$ the parameters are determined as $a = 664$ MeV and $b = 0.03\,\Lambda^3$ to give a deconfinement transition temperature of $T_c = 270$ MeV in the pure gauge case and of about $T = 200$ MeV in the presence of quarks.

A comparison of those potentials is shown in [31]. Below T_c these three potentials essentially agree. Above, $\mathcal{U}_{\text{poly}}$ and $\mathcal{U}_{\log}$ approach the Stefan-Boltzmann pressure limit whereas $\mathcal{U}_{\text{Fuku}}$ does not. It is argued that starting at about $2T_c$ transverse gluons should make up the most relevant contribution to the pressure [31]. However they are not included in the model.

The Polyakov loop potentials correctly reproduce the behavior of the Polyakov loop in the pure gauge limit of QCD: Below T_c the potentials have a single minimum at $\Phi = 0$ which is $\mathbb{Z}_3$ symmetric. At high temperatures three degenerate minima develop at nonzero Φ which are connected by $\mathbb{Z}_3$ transformations. Above T_c these minima are the absolute minima of the potential, thus the $\mathbb{Z}_3$ symmetry is spontaneously broken.

For the first part of this work we will stick to the polynomial form $\mathcal{U}_{\text{poly}}$ with parameters given in Table 2.2. We changed T_0 to 190 MeV. This makes the chiral and deconfinement phase transition happen at lower temperatures which are closer to existing lattice QCD results. The transition temperatures at $\mu = 0$ from lattice simulations with $2{+}1$ flavors range from $146 - 170$ MeV [4] to $185 - 195$ MeV [35]. Rescaling is also justified since T_0 is found to depend on the number of quark flavors [36].

a_0	a_1	a_2	a_3	b_3	b_4	T_0 in MeV
6.75	−1.95	2.625	−7.44	0.75	7.5	190

Table 2.2: Parameter choice (Polyakov loop part), taken from [34]. T_0 has been reduced from 270 MeV.

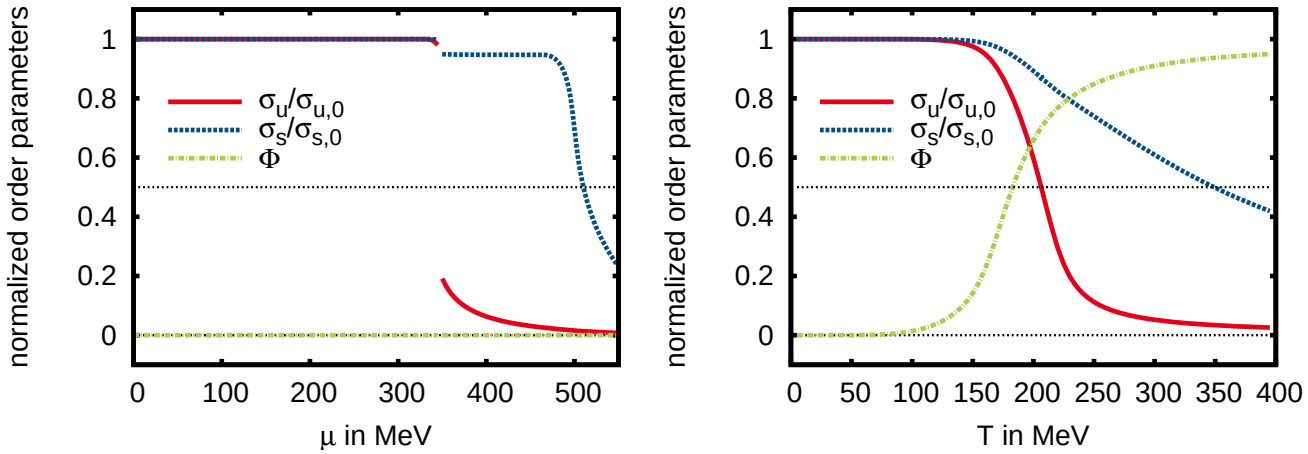

Figure 2.1: The chiral condensates and the Polyakov loop expectation value at $T = 0$ as a function of μ (left) and at $\mu = 0$ as a function of T (right). The chiral condensates are normalized by their vacuum values. The value 0.5, which can be used as a crossover criterion, is shown as an eye guide.

2.3 Phase transitions and the phase diagram

In Fig. 2.1 we show the behavior of the order parameters of chiral symmetry and deconfinement at the μ- and T-axis.

With the present parameter set we find the following results:

At $T = 0$, see left plot of Fig. 2.1, the chiral condensates have a discontinuity at $\mu = 345$ MeV. The light quark condensate drops to a low value which indicates that chiral symmetry for the light quark flavors is approximately restored. The strange quark condensate drops only slightly at that point, but at about 500 MeV a steep continuous decrease takes place. This is considered as a crossover transition. The Polyakov loop expectation value is always zero along the μ-axis.

There is not a unique definition for the crossover temperature/chemical potential. Straightforward criteria are e. g. a) the position where the normalized order parameter crosses the value 0.5, b) the position of the maximum of the temperature/chemical potential derivative of the order parameter, or c) the position of the maximum of the respective susceptibility. For simplicity we will at the moment restrict the discussion to case a). This issue will be addressed in more detail in a later chapter.

At $\mu = 0$ we find crossover transitions only, compare right plot of Fig. 2.1. The Polyakov loop rises from 0 to 1 whereas the chiral condensates drop smoothly from their vacuum value down to about zero. The strange quark chiral crossover transition sets in later and is much slower than the light quark one. The crossover temperatures are $T_{0,ud} = 206.5$ MeV, $T_{0,s} = 349$ MeV and $T_{0,dec} = 183$ MeV for chiral and deconfinement transitions respectively.

Fig. 2.2 represents the phase diagram of the three-flavor PNJL model in the $\mu - T$ plane.

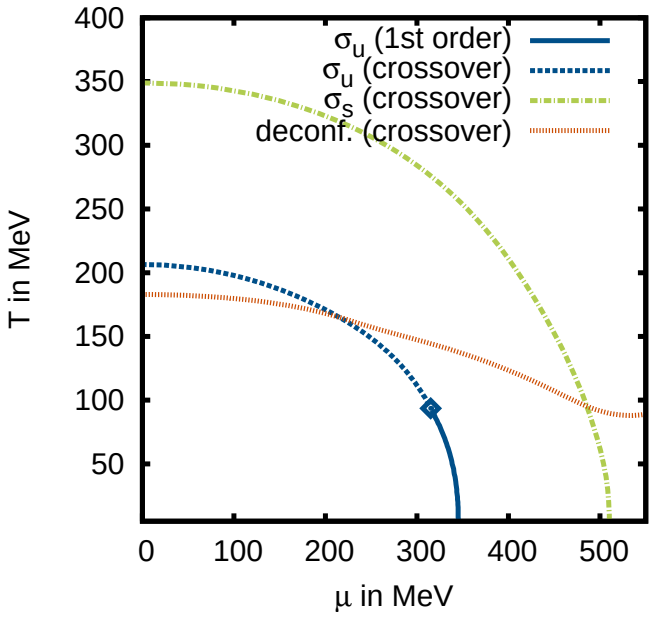

Figure 2.2: The phase diagram in the PNJL model for real μ. The chiral first order transition is shown as a solid curve whereas crossover transitions are visible in a dashed style. The critical endpoint is also shown.

The first order chiral phase transition starting on the μ-axis continues to non-zero temperature with lower chemical potential and ends in a critical point at $T_c = 94$ MeV, $\mu_c = 315$ MeV.

The deconfinement transition is determined using the geometric mean of the real valued Polyakov loop expectation values $\sqrt{\Phi\bar{\Phi}}$ for conformity with later comparison.

3 The PNJL model at imaginary chemical potential

In this chapter we will introduce the PNJL model with imaginary quark chemical potential, following Sakai et al. In [23] the PNJL model with imaginary quark chemical potential in the chiral limit using the polynomial Polyakov loop potential is investigated. The study is extended to finite bare quark masses in [24] where also an eight-quark interaction is added. A comparison to lattice results is performed in [26], where the logarithmic potential is employed. The mechanism that leads to discontinuities at high temperatures is analyzed in [27] using the Polyakov loop potential by Fukushima.

3.1 The extended $\mathbb{Z}_3$ symmetry

The pure gauge limit of QCD is symmetric under a $\mathbb{Z}_3$ transformation which can be characterized as a rotation of the (complex) Polyakov loop,

$$\Phi \quad \rightarrow \quad \Phi \exp\left[-i2\pi k/3\right] \quad \text{with} \quad k \in \mathbb{Z}. \tag{3.1}$$

This symmetry is lost when dynamical quarks are added to the system. In 1986, Roberge and Weiss (RW) [12] found out that QCD with an imaginary chemical potential

$$\mu = i\theta T \tag{3.2}$$

is periodic in θ with a period of $2\pi/3$ when at the same time a $\mathbb{Z}_3$ transformation is applied.

The combination of the $\mathbb{Z}_3$ transformation and a shift in the imaginary chemical potential

$$\begin{aligned} \Phi \quad &\rightarrow \quad \Phi \exp\left[-i2\pi k/3\right] \\ \theta \quad &\rightarrow \quad \theta + 2\pi k/3 \end{aligned} \tag{3.3}$$

is called the "extended $\mathbb{Z}_3$ transformation". Note that "extended" might be misleading since the transformation is more restrictive than the common $\mathbb{Z}_3$ transformation. This is an extension of the $\mathbb{Z}_3$ transformation to a system with quarks.

We want to show that the thermodynamic potential of the PNJL model is invariant under the extended $\mathbb{Z}_3$ transformation. The Polyakov loop expectation values Φ and $\bar{\Phi}$ themselves are not invariant under the extended $\mathbb{Z}_3$ transformation. We thus introduce the more convenient "modified Polyakov loop" and its complex conjugate

$$\Psi = \Phi e^{i\theta} \qquad \bar{\Psi} = \bar{\Phi} e^{-i\theta} \tag{3.4}$$

which are then invariant under the extended $\mathbb{Z}_3$ transformation,

$$\Psi = \Phi e^{i\theta} \quad \rightarrow \quad \Phi e^{-i2\pi k/3} e^{i\theta + 2\pi k/3} = \Psi. \tag{3.5}$$

As soon as we allow Φ, $\bar{\Phi}$ or Ψ, $\bar{\Psi}$ to become complex, we need to impose the condition that they are related by complex conjugation, otherwise the thermodynamic potential would become complex. As we are at imaginary chemical potential the connection to the free energy (eq. (2.5)) is already invalid, hence the Polyakov loop does not need to be constrained to real values. In our numerical implementation we represent the modified Polyakov loop by its absolute value $|\Psi|$ and its phase $\arg(\Psi)$ for which the following relations hold:

$$|\Psi| = \sqrt{\Psi\bar{\Psi}} = \sqrt{\Phi\bar{\Phi}} = |\Phi| \qquad \arg(\Psi) = \arg(\Phi) + \theta. \tag{3.6}$$

We can then express the thermodynamic potential in terms of the modified Polyakov loop:

$$\begin{aligned}\Omega(T,\theta;\sigma_f,\Psi) = -2\sum_f \int \frac{d^3p}{(2\pi)^3}\Bigg\{ & N_c E_f(p) \\ & + T\log\left[1 + 3\Psi e^{-\frac{E_f}{T}} + e^{i3\theta}\left(3\bar{\Psi}e^{-2\frac{E_f}{T}} + e^{-3\frac{E_f}{T}}\right)\right] \\ & + T\log\left[1 + 3\bar{\Psi} e^{-\frac{E_f}{T}} + e^{-i3\theta}\left(3\Psi e^{-2\frac{E_f}{T}} + e^{-3\frac{E_f}{T}}\right)\right]\Bigg\} \\ & + g_S(\sigma_u^2 + \sigma_d^2 + \sigma_s^2) + 4g_D\sigma_u\sigma_d\sigma_s + \mathcal{U}_{\text{Polyakov}}(\Psi,\bar{\Psi},T,\theta)\end{aligned} \tag{3.7}$$

and we continue to use the polynomial Polyakov loop potential (2.14) which then becomes

$$\frac{\mathcal{U}_{\text{poly}}}{T^4} = -\frac{b_2(T)}{2}|\Psi|^2 - \frac{b_3}{3}|\Psi|^3\cos\left(3\arg(\Psi) - 3\theta\right) + \frac{b_4}{4}|\Psi|^4. \tag{3.8}$$

The Polyakov loop potentials are invariant under the $\mathbb{Z}_3$ transformation and also under the extended $\mathbb{Z}_3$ transformation as they are independent of the chemical potential. As the thermodynamic potential is now written in terms of the invariant quantities $\Psi(\theta)$, $\sigma_f(\theta)$, $e^{\pm i3\theta}$ and $\cos\left(3\arg(\Psi) - 3\theta\right)$ only, it is obvious that it is invariant under the extended $\mathbb{Z}_3$ transformation.

3.2 Roberge-Weiss periodicity and phase transition

From the invariance of the thermodynamic potential and the modified Polyakov loop under the extended $\mathbb{Z}_3$ transformation, it follows that the stationary conditions for $\Psi(\theta)$ and $\Psi(\theta + 2\pi k/3)$ are the same. This effects

$$\Psi\left(\theta + \frac{2\pi k}{3}\right) = \Psi(\theta). \tag{3.9}$$

If we plug the solutions of the gap equations $\Psi(\theta)$, $\sigma_f(\theta)$ back into (3.7) we obtain the thermodynamic potential in terms of T and θ only:

$$\Omega(T,\theta) = \Omega\left(T,\theta;\sigma_f(T,\theta),\Psi(T,\theta)\right) \tag{3.10}$$

and we finally have the periodicity of the thermodynamic potential

$$\Omega\left(T,\theta + \frac{2\pi k}{3}\right) = \Omega(T,\theta). \tag{3.11}$$

order parameter		symmetry w.r.t. θ
light quark condensate	σ_{ud}	even
heavy quark condensate	σ_s	even
modified Polyakov loop	$\lvert\Psi\rvert$	even
	$\arg(\Psi)$	odd
	$\mathrm{Re}(\Psi)$	even
	$\mathrm{Im}(\Psi)$	odd

Table 3.1: Symmetry properties of the order parameters

This is the so called Roberge-Weiss (RW) periodicity in the imaginary chemical potential region that occurs for all temperatures. We will consider a period to be $0 \leq \theta \leq 2\pi/3$.

Through the stationary conditions (2.10) we find relations for the order parameters:

$$\Psi(\theta) = \bar{\Psi}(-\theta) \qquad \text{and} \qquad \sigma_f(\theta) = \sigma_f(-\theta). \tag{3.12}$$

This immediately translates into the symmetry properties summarized in Tab. 3.1.

In the aforementioned interval θ-even (θ-odd) quantities with the RW periodicity will be symmetric (anti-symmetric) with respect to the line at the middle of the interval, $\theta = \pi/3$. Moreover all θ-odd quantities with the RW periodicity will be discontinuous at each $\theta = \pi/3 \mod 2\pi/3$ unless their value is zero at that point. This discontinuity is called the RW phase transition and is of first order. θ-even quantities with the RW periodicity will have a discontinuous θ-derivative at each $\theta = \pi/3 \mod 2\pi/3$ unless the derivative itself is zero at that point.

The connection between discontinuities appearing in different quantities has been investigated thoroughly in [25]. The authors extend a theorem about relations among first order phase transitions (zeroth order discontinuities, i. e., jumps, of the order parameters) [37] to first order discontinuities (i. e., cusps) and apply it to the PNJL model at imaginary chemical potential. It explains that since the position of the RW transition lines at $\mu = (2k+1)\pi/3$ does not depend on external quantities the zeroth order discontinuity in $\frac{\partial\Omega}{\partial\theta}$ propagates to θ-odd quantities as zeroth order discontinuities but to θ-even quantities as first order ones.

The RW periodicity and transition can be observed in PNJL model calculations. We will now show that all abovementioned possibilities are existent for different quantities and different temperature regimes. In Fig. 3.1 we present results at two different temperatures, $T = 170$ MeV and $T = 220$ MeV, below and above $T_{RW} = 206$ MeV. The order parameters of the chiral and deconfinement transitions and the thermodynamic potential are shown as functions of θ. Only one period is shown since all quantities have the RW periodicity. The imaginary part and the phase of the modified Polyakov loop are odd with respect to θ as expected whereas all other presented quantities are even functions. Discontinuities only appear on the RW transition line. At high temperature the odd quantities have a discontinuity, and even quantities (except $\mathrm{Re}(\Psi)$) show a cusp. At low temperatures all quantities are smooth.

The origin of the RW phase transition at high temperatures is the following: In the case of QCD without quarks (pure gauge case) the deconfinement phase transition along the temperature axis occurs at $T_c = 270$ MeV and is of first order. Below T_c only one ground state exists, which is $\mathbb{Z}_3$ symmetric. For temperatures higher than T_c there are three degenerate ground states, so the $\mathbb{Z}_3$ symmetry is spontaneously broken. Including quarks the $\mathbb{Z}_3$ ground states are modified but

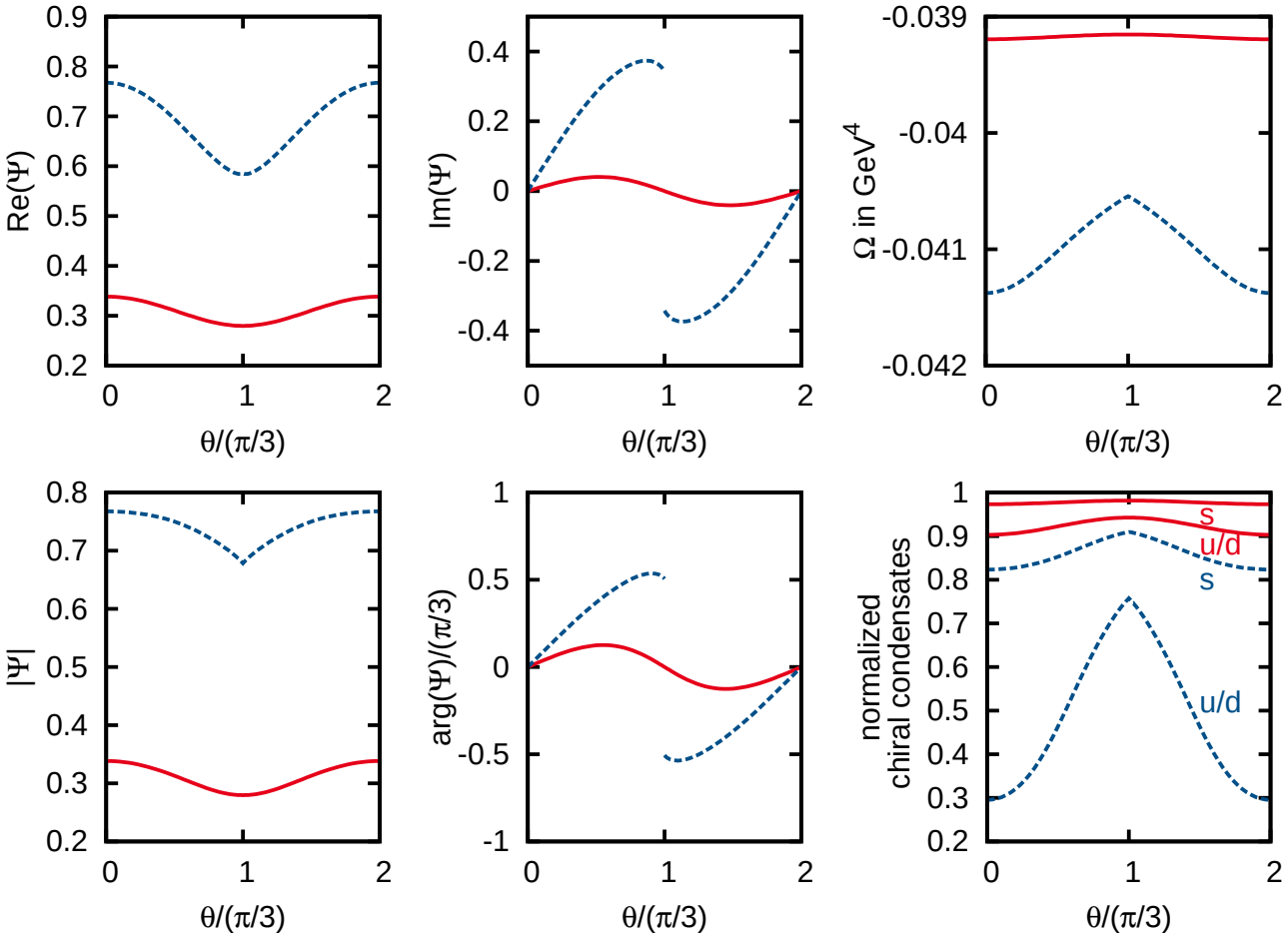

Figure 3.1: Dependence of the thermodynamic potential (top right), the chiral condensates of up/down and strange quarks (bottom right) and the modified Polyakov loop (others) on θ for temperatures below T_{RW} (170 MeV, solid red lines) and above T_{RW} (220 MeV, dashed blue lines). $T_{RW} = 206$ MeV in this case.

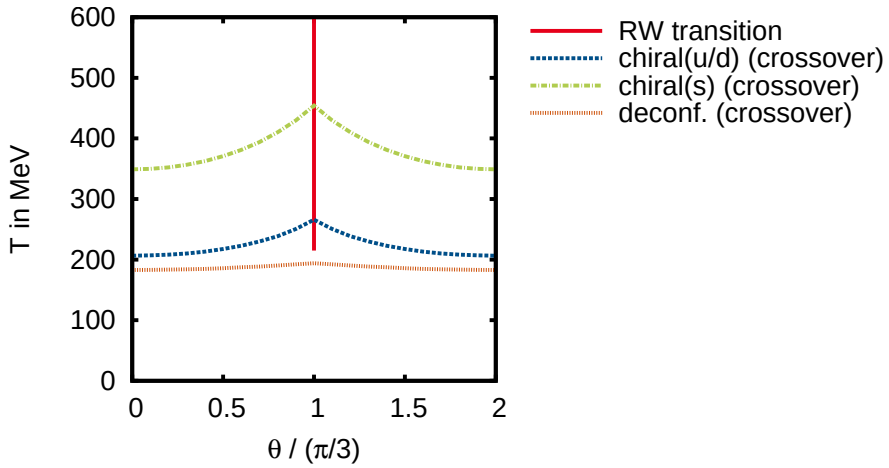

Figure 3.2: Phase diagram in the imaginary chemical potential region

still present as $\mathbb{Z}_3$ sectors which can be characterized by the Polyakov loop phase. Above T_{RW} there are three $\mathbb{Z}_3$ sectors and transitions from one to another happen at $\theta = \pi/3 \mod 2\pi/3$. At each RW transition line two $\mathbb{Z}_3$ sectors are equivalent. Below T_{RW} the transition takes place continuously. Refer to [12] for a perturbative and strong coupling QCD analysis and [27] for an analysis of the "RW mechanism" in the PNJL framework.

3.3 Phase diagrams

In the $\theta - T$ plane we determine the phase diagram. The first period is shown in Fig. 3.2. The same crossover criterion as before in the real chemical potential region (normalized order parameter $= 0.5$) is applied to the chiral condensates and the modified Polyakov loop . Remember that $|\Psi| = |\Phi| = \sqrt{\Phi\bar{\Phi}}$ which was used as the deconfinement order parameter in the previous chapter. From that we find the crossover transition lines shown in dashed style. Furthermore we show the first RW transition line at $\theta = \pi/3$ which starts at $T_{RW} = 206$ MeV (temperature value valid for all RW transition lines).

On the RW transition lines there is a first order phase transition in the phase of the modified Polyakov loop. The chiral condensates have a cusp (discontinuity in the θ-derivative), however the susceptibilities do not diverge. In the present case the endpoint of the RW transition at T_{RW} is of second order. The order of the endpoint will be central topic of Chapter 5. A similar phase diagram (without the strange quark crossover line and with a different parameter set) has been found in a $N_f = 2$ PNJL model analysis [24].

As we have determined the phase diagrams in the $\mu - T$ and $\theta - T$ planes we are able to display the results in a merged phase diagram in the $\mu^2 - T$ plane, see Fig. 3.3. The periodicity is not obvious in this plot any more. For orientation the start of the second RW transition line is visible at the left border. We observe that the crossover transition lines are analytic at $\mu^2 = 0$. This is essential for our aim to perform extrapolations of crossover transition lines from $\mu^2 < 0$ to $\mu^2 > 0$ which will be covered in the upcoming chapter.

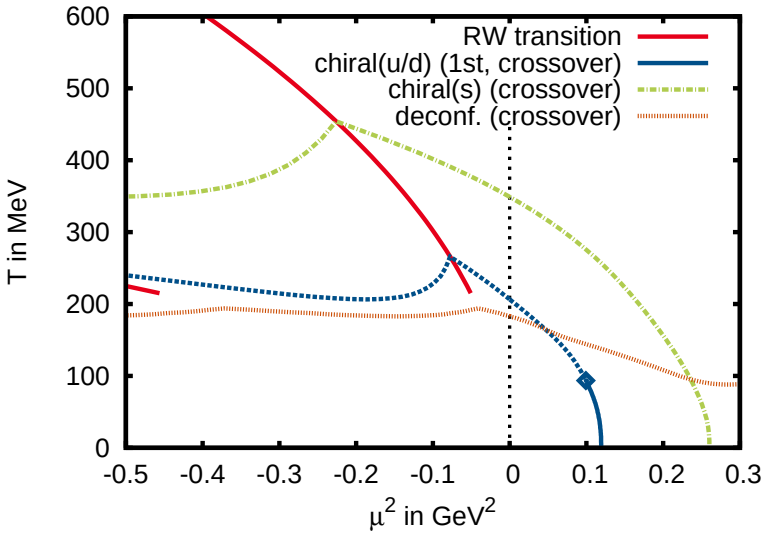

Figure 3.3: Phase diagram in the $\mu^2 - T$ plane.

4 Extrapolation of chiral crossover transition lines

4.1 Introduction

Now that we have identified the transition lines in the real and imaginary chemical potential regions, we are ready to perform an extrapolation of the results from imaginary to real chemical potential.

In the $T-\mu^2$ plane the transition from imaginary chemical potential ($\mu^2 < 0$) to real chemical potential ($\mu^2 > 0$) is analytic. We are thus able to fit to data points obtained at $\mu^2 < 0$ and continue the line to the real chemical potential region at $\mu^2 > 0$.

For the following analysis we will consider the light quark chiral phase transition only. Of course these fits and extrapolations can be performed in the same way for the deconfinement and strange quark chiral crossover transition lines. As the transition is continuous in the considered region, we first of all need to deal with different crossover criteria.

4.2 Crossover criteria

For the chiral phase transitions the chiral condensates σ_f are the order parameters. The absolute value of the Polyakov loop expectation value ($|\Phi| = \sqrt{\Phi\bar{\Phi}} = \sqrt{\Psi\bar{\Psi}} = |\Psi|$) is used as an order parameter for the deconfinement phase transition.

We will restrict the definitions on the light quark chiral phase transition, as the definitions for the strange quark chiral phase transition and deconfinement phase transition work accordingly.

In the previous chapter we already used a very simple definition of the chiral crossover transition, namely

$$\frac{\sigma_{ud}(T,\mu)}{\sigma_{ud,0}} = 0.5 \tag{4.1}$$

with the vacuum value $\sigma_{ud,0} \equiv \sigma_{ud}(T=0,\mu=0)$. It will be denoted as criterion "A" in the following. This naive definition gives a rough estimate for the transition temperature only. It does not necessarily coincide with the correct position of the discontinuity at a first or second order phase transition. For the deconfinement crossover transition the order parameter is normalized by the asymptotic value at high temperatures, which is 1 for the Fukushima and logarithmic potentials and slightly larger than one for the polynomial Polyakov loop potential.

An improved definition uses the inflection point of the order parameter along lines of constant chemical potential (criterion "B"). This is equivalent to the maximum in the temperature derivative of the order parameter

$$\max\left(\frac{d\sigma_{ud}}{dT}\right)_{\mu}. \tag{4.2}$$

This definition does give the correct position of a second order phase transition.

The peak position of the light quark chiral susceptibility (criterion "C") given by

$$\chi_{chiral} = \frac{\partial^2(-\Omega/T)}{\partial m_{ud}^2} = -\frac{1}{T}\frac{\partial \sigma_{ud}}{\partial m_{ud}} \tag{4.3}$$

is the most reasonable criterion. The chiral susceptibility diverges at a second order chiral phase transition, for instance at the endpoint of the first order chiral phase transition in the real chemical potential region, and shows a peak along the crossover transition [38, 31]. Derivatives of the mean fields must be taken into account. Since we use a difference quotient to calculate the derivative these contributions are included.

In Fig. 4.1 we compare the three crossover criteria for each of the three Polyakov loop potentials. The parameters for the different Polyakov loop potentials have already been given in section 2.2. As before, parameter T_0 has been reduced to 190 MeV for the polynomial and logarithmic potentials to reduce the transition temperatures. Since the parameter set for the Fukushima potential is unchanged, the transition temperatures are higher than in the cases of the polynomial and logarithmic parameterizations.

For almost the whole interval of μ^2 the curves are ordered like $T_A < T_B < T_C$. The largest deviations between the curves $(T_C - T_A)$ of about 15-20 MeV are found in the imaginary chemical potential region. The ordering and the spacing between the curves is nearly independent of the chosen Polyakov loop potential.

In the critical endpoint all lines join together, and already at some lower chemical potential they come closer together as the transition is more rapid in the vicinity of the second order endpoint.

At real chemical potentials curves belonging to criterion B show a dip in the case of the polynomial and logarithmic potentials. The dip is more pronounced in the latter version and nonexistent for the Fukushima one. It originates from the influence of the deconfinement transition which lies below the chiral transition. With the Fukushima potential both transitions are rather close together. For the other two potentials the transition is about 40 MeV apart (according to criterion B in each case) at $\mu = 0$. The rise of the Polyakov loop at the deconfinement crossover transition influences the chiral condensate by lowering it. This is visible as an additional narrow peak in the temperature derivative of the chiral condensate and thus affects criterion B for the chiral crossover transition. The two peaks merge close to the chiral endpoint. As the run of the curve including the dip is rather complicated, criterion B is not adequate for the extrapolation. Curves associated to criteria A and C do not have that complicated structure and are thus considered for the extrapolation.

4.3 Extrapolation method

Data points of the chiral crossover line at imaginary chemical potential will be fit to a polynomial ansatz as given by

$$T_c(\mu^2) = \sum_{i=0}^{n} a_i \, (\mu^2)^i. \tag{4.4}$$

The order of the polynomial will be varied from $n = 2$ to $n = 6$.

We use a nonlinear least-squares Marquardt-Levenberg fitting algorithm provided by *gnuplot* (version 4.5).

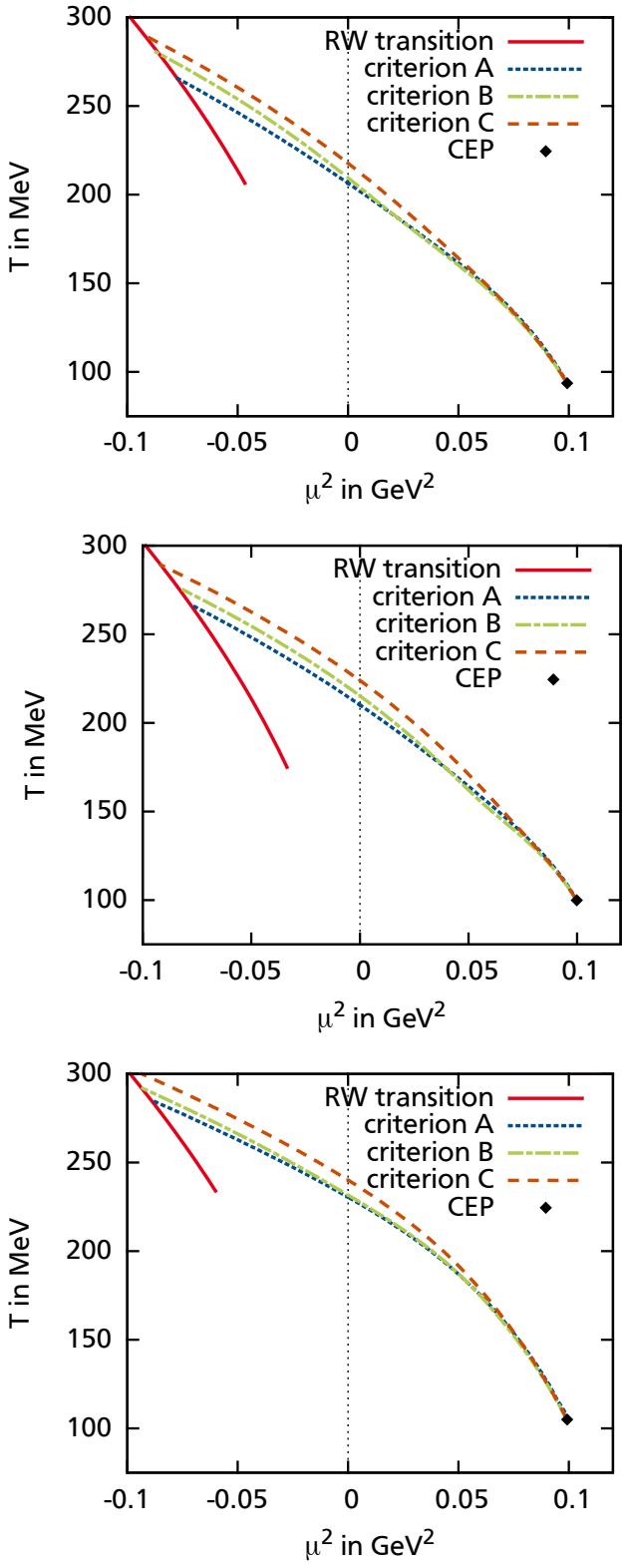

Figure 4.1: Chiral crossover transition lines in the $\mu^2 - T$ plane for different crossover criteria. The polynomial/logarithmic/Fukushima Polyakov loop potential has been used in the top/middle/bottom picture. Regularization scheme II has been applied in all cases. See text for details.

As input for the fitting procedure we use 60-100 data points in the imaginary chemical potential region starting at $\mu = 0$ and ending on the first RW transition line at $\theta = \pi/3$, where the chiral condensate has a first order discontinuity (cusp).

Extrapolations to the real chemical potential region are obtained by plugging positive values of μ^2 into the resulting polynomials.

The input data are precise up to numerical uncertainties in the determination of the crossover criterion smaller than $\Delta T = 0.05$ MeV. In the plots we will add error bands stemming from a Gaussian error propagation taking into account the error estimates Δa_i that are output by the fitting algorithm for each coefficient.

$$\Delta T_c(\mu^2) = \sqrt{\sum_{i=0}^{n} \left(\Delta a_i \, \mu^{2i}\right)^2} \tag{4.5}$$

Error bands will be omitted if the corresponding line is thicker than the error band.

4.4 Results

First, we carefully checked that the different crossover transition lines are continuous at the change from imaginary to real chemical potential. The calculations at both sides of the $\mu^2 = 0$ axis give the same result in the limit of vanishing chemical potential. Moreover, the data points in the immediate vicinity of $\mu^2 = 0$ perfectly fit to the same linear behavior on both sides. Thereby we excluded that the different treatments of the Polyakov loop in the two regimes produces deviations in leading order of μ^2.

As examples of our study we present in Figure 4.2 extrapolations of the chiral crossover line using crossover criteria A, B and C for the polynomial Polyakov loop potential and regularization II, denoted as setup 1-3.

Setup 1

Second and third order lines of this setup are almost identical. Both perfectly reproduce the almost linear part of the line up to $\mu^2 = 0.06$ GeV^2. At higher μ^2 the bend is not picked up. Higher order lines move away from the correct curve.

Setup 2

In setup 2 the extrapolations are able to describe the course of the crossover transition with increasing agreement for higher order polynomials. However, the good description is limited by the position of the dip which was discussed before. Beyond the dip the fifth and sixth order lines bend into the wrong direction.

Setup 3

The extrapolation using criterion C provides a very good description of the direct calculation with small improvements from second to fifth order. The sixth order line is not very far off but has notably larger errors.

Due to the good performance of criterion C in the current comparison, we will stick to it for the next comparison where we now want to contrast extrapolations using different Polyakov

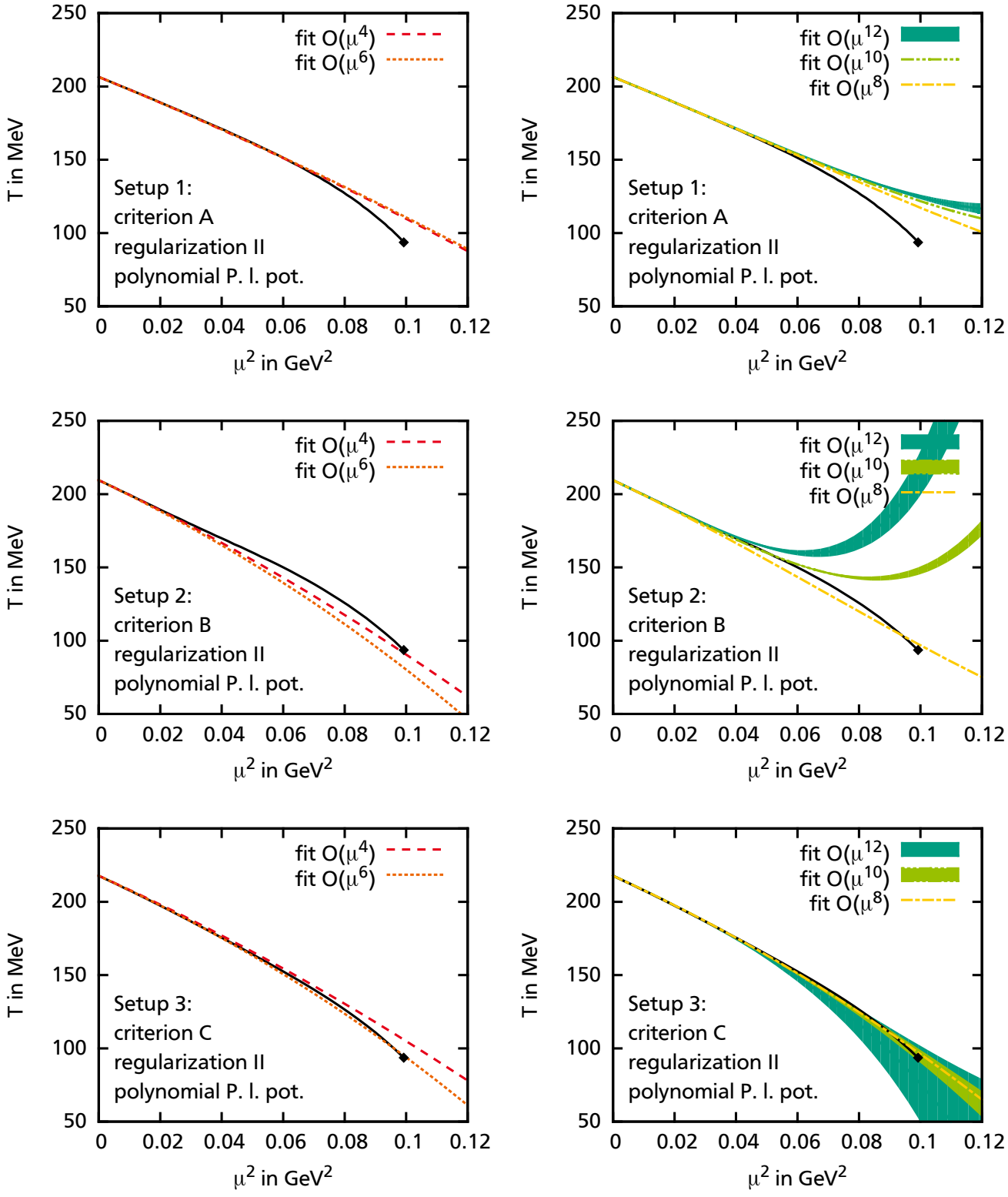

Figure 4.2: Extrapolations using different crossover criteria for the polynomial Polyakov loop potential (P. l. pot.) and regularization II. Quadratic and cubic polynomials are shown on the left side, higher order polynomials on the right side. Direct calculations of the respective crossover line and the critical endpoint are shown in solid style. Error bands are omitted when they are thinner than the current line.

loop potentials and regularizations. In our next figure, 4.3, we first analyze the logarithmic and the Fukushima potentials, while still employing regularization scheme II (setups 4 and 5). We then switch exemplarily to regularization scheme I while employing the polynomial Polyakov loop potential (setup 6).

Setup 4 & 5

The behavior in setup 4 and 5 is very similar to setup 3: Going from the second to the fifth order polynomial gives a continuous improvement for the extrapolation. The sixth order polynomial however has large uncertainties and moves away from the correct line. The agreement in setup 5 is not as good as in setup 4, this can be explained by the stronger bending of the curve in the Fukushima case.

Setup 6

In setup 6 big changes occur between different orders with no apparent convergence. Even at small μ^2 the low order lines deviate notably from direct calculations. We find an astonishingly good agreement of the fifth order extrapolation. It follows the directly calculated curve up to high μ^2 and is even pretty close to the critical endpoint. The fourth and sixth order lines, however, are far off.

4.5 Discussion

Finally, we want to summarize our observations on the extrapolations. As expected, criterion B is not suitable for an extrapolation. Our favorite description of the chiral crossover transition is the peak of the chiral susceptibility (criterion C).

In the majority of cases low order curves match the overall run of the curve as can be expected for lines without complicated structure. The almost linear behavior of the crossover lines for small μ^2 is well reproduced in most cases, whereas the bending at higher μ^2 is not. Very rarely the critical endpoint is well approximated by an extrapolated curve or enclosed by their error bands. Extrapolations using polynomials of order five and higher in μ^2 have large errors bands. Surprisingly, in all cases with criterion C order five results are in good agreement with the direct calculation whereas the inclusion of terms of order six is disadvantageous. In some cases the position of the curves fluctuates strongly when going from one order to the next.

We conclude that extrapolations using polynomial fit functions do not reliably reproduce the direct calculations at real chemical potentials. Choosing different fit functions might improve the extrapolations. More sophisticated ansätze could take into account the periodicity in the $\mu - T$ plane (which has to be translated to a μ^2 dependence appropriately). The oscillatory behavior could be cured by using Padé approximants instead of simple polynomials.

In lattice QCD calculations considerably less data points are available which additionally contain statistical errors. While the determination of the crossover transition line curvature at $\mu^2 = 0$ might be possible, the determination of the course of the line up to the endpoint seems impossible under present conditions.

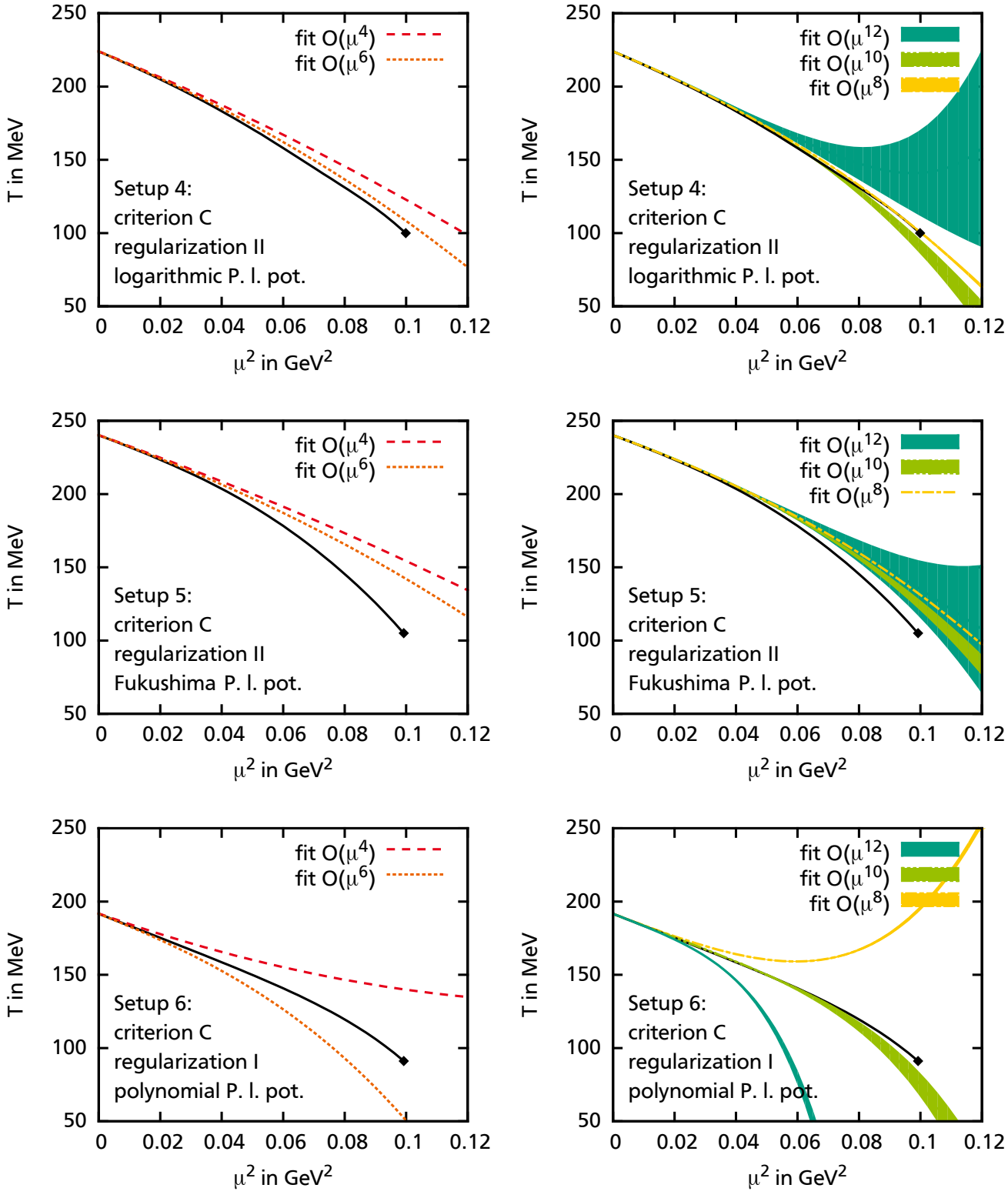

Figure 4.3: Top and middle row: Extrapolations using crossover criterion C for the logarithmic and Fukushima Polyakov loop potentials (P. l. pot.) and regularization II. Bottom row: Extrapolations using crossover criterion C for the polynomial Polyakov loop potential and regularization I. See caption of previous figure and text for more information.

5 The order of the Roberge-Weiss transition endpoint

5.1 Introduction

In a recent publication D'Elia and Sanfilippo studied the order of the RW endpoint in two-flavor lattice QCD [28]. Via a finite size scaling analysis they find that the point is first order for low and high quark masses and of second order for intermediate quark masses. They discuss phenomenological consequences. In the case of a first order (triple) point, first order lines will depart from it. One of those lines could reach up to the $\theta = 0$ axis or even cross it, extending into the real chemical potential region. It would end in a second order endpoint and join up with the deconfinement crossover transition.

A short time ago Philipsen [29] presented preliminary results for $N_f = 3$ which support the findings at $N_f = 2$: there is a first order transition at low and high quark masses which weakens to second order in between.

The RW endpoint has also been studied in the PNJL model with two flavors [27]. Using the Fukushima potential (with $b = 0.015\,\Lambda^3$ such that the deconfinement crossover transition at vanishing chemical potential is approximately at $T = 180$ MeV) Kouno et al. find the RW endpoint to be of second order. We discovered that in a previous paper by the same group [26] where the logarithmic Polyakov loop potential was used (with $T_0 = 212$ MeV) it is visible in Fig. 5 that the RW endpoint is of first order. However, the authors did not comment on it.

Why do different Polyakov loop potentials give such different results on the order of the RW endpoint? We will show, that the relative strength of the "gluonic" to the "quark" contributions to the thermodynamic potential determines the order of the endpoint.

Remember that in the pure gauge limit the deconfinement phase transition occurs at $T_c = 270$ MeV and is of first order. When the "gluonic" degrees of freedom have a large contribution to the thermodynamic potential through the Polyakov loop potential, the RW endpoint will be of first order. When the quark contributions are dominating instead, the transition is of second order.

To confirm this we need to adjust this relative strength. In the PNJL model this can be done in two ways: the first is increasing the bare quark mass m_0 which suppresses the influence of the quarks to the pressure. Note that this changes properties like the pion mass and decay constant to which the original parameter set was fitted. The second way is to directly change the weight of the Polyakov loop potential in the thermodynamic potential. This is particularly simple for the Fukushima potential where b is an overall factor.

5.2 Model setup

In order to compare to previous results and to perform the analysis described in the last section, we will choose a somewhat different environment: we restrict the model to two degenerate

Λ in MeV	m_0 in MeV	$g_S\Lambda^2$
631.5	5.5	4.385

Table 5.1: Parameter choice (NJL part) for the two-flavor PNJL model, taken from [26].

quark flavors $N_f = 2$. This matches the aforementioned work of Kounu, Sakai et al. [26, 27] in the PNJL model and fits to Lattice calculations of D'Elia and Sanfilippo [28]. In addition we thus have only one bare quark mass $m_0 \equiv m_u = m_d$ left that can easily be modified.

Necessary modifications to the initially described $N_f = 2 + 1$ PNJL model can be outlined by: sum over degenerate up and down quarks only and leave out the 't Hooft term ($g_D = 0$). We use parameters given in [26], shown in Table 5.1.

5.3 Results

In the upcoming sections we will present results of calculations with the logarithmic and the Fukushima Polyakov loop potentials. In each case we will first repeat the calculations by Kounu, Sakai et al. [26, 27] and then perform further analyses.

For the logarithmic potential, where the order of the RW transition endpoint will be of first order, we will investigate the implications of the first order transition. Furthermore some model parameters will be altered and finally the dependence on the bare quark mass will be studied.

After that, we examine the model while employing the Fukushima potential. Mainly the parameter b will be varied and resulting changes are discussed.

5.3.1 Logarithmic Polyakov loop potential

As announced before, we will first repeat and extend calculations seen in [26]. The logarithmic Polyakov loop potential is used with parameters given in Section 2.2, T_0 is changed to 212 MeV to reduce the pseudo-critical temperature.

Fig. 5.1 shows the behavior of the order parameters with respect to temperature along the first RW transition line ($\theta = \pi/3$). The left pane of our Figure 5.1 corresponds to parameter set A of Fig. 5(a) in [26]. We find that all quantities are discontinuous at $T_{RW} = 190.3$ MeV, especially the phase of Ψ shows a big jump. On the RW transition line above T_{RW} positive and negative values of the modified Polyakov loop phase are degenerate, $\arg(\Psi) \longleftrightarrow -\arg(\Psi)$ (only the positive value is shown in the figure). Discontinuities in the modified Polyakov loop have an impact on chiral quantities. The discontinuity in the chiral condensate is small but clearly visible. This behavior is clear evidence for a first order transition at the endpoint of the RW phase transition.

As we expect first order transition lines departing from the first order endpoint, we investigated the area around the endpoint in more detail. The dependence of the aforementioned quantities on the imaginary chemical potential is depicted in Fig. 5.2. Curves for three different temperatures around T_{RW} are displayed. Above T_{RW} the absolute value of Ψ and the chiral condensate have a cusp at $\theta = \pi/3$ and the phase of Ψ jumps from its positive to negative value as shown before in Fig. 3.1. At low temperature all quantities are continuous. In between, a new

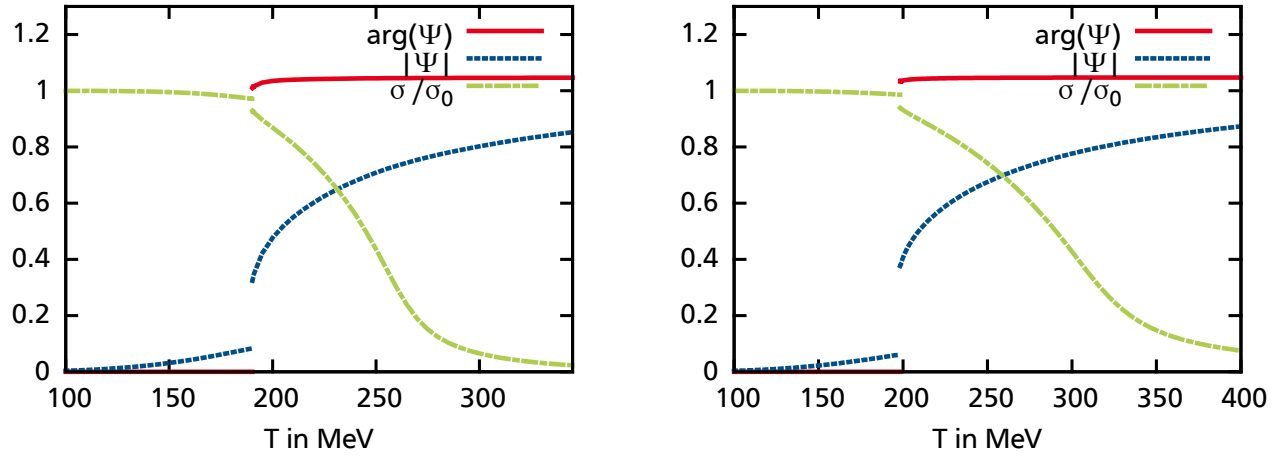

Figure 5.1: Modified Polyakov loop phase and absolute value as well as the normalized chiral condensate at $\theta = \pi/3$ as function of temperature. Left side uses regularization scheme I, right side uses regularization scheme II.

behavior is observed. Again, the quantities are discontinuous: in the vicinity of $\theta = \pi/3$ the system jumps to a lower value of $|\Psi|$ (confined phase). Since $|\Psi|$ and σ are even functions and $\arg(\Psi)$ is an odd function with respect to $\theta = \pi/3$ the discontinuity appears on both sides of the RW transition line.

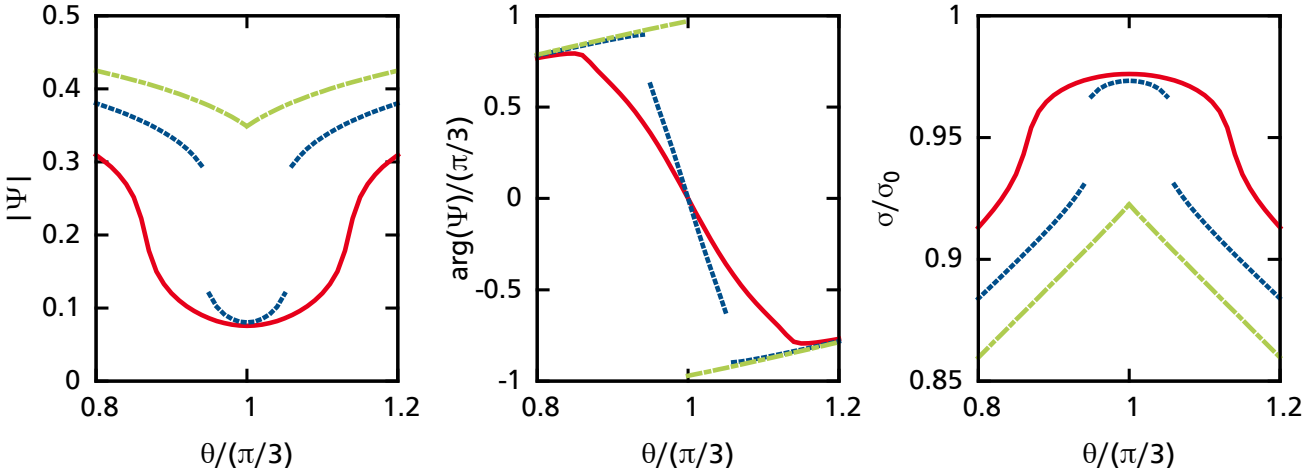

Figure 5.2: Dependence of the modified Polyakov loop and the normalized chiral condensate on θ for different temperatures around $T_{RW} = 190.3$ MeV (solid: $T = 185$ MeV, dashed: 188 MeV, dot-dashed: 191 MeV).

To back our finding we calculate the potential surface at the end of the RW transition line. For chosen points in the phase diagram (T, θ) and a fixed modified Polyakov loop phase $\psi = \arg(\Psi)$ we find the minimal solution to the gap equations. This defines the potential surface $\Omega(T, \theta; \psi)$. ψ can be treated as an order parameter of the RW transition as it is an odd function with respect to $\theta = \pi/3$. Results are presented in Fig. 5.3. The vacuum potential $\Omega(T = 0, \theta = 0)$ has been subtracted in this case. We show the situation along the RW transition line for various temperatures. At small temperatures there is a single minimum at $\psi = 0$. For high temperatures there are two minima at about $\psi = \pm\pi/3 \approx 1.05$. In between is the interesting region around temperatures of T_{RW}. Approaching the RW transition line from below, the minimum at $\psi = 0$ becomes deeper and flatter. Eventually, two dips emerge at $\psi \approx \pm 1.05$ which at a temperature higher than T_{RW} are deeper minima than the center one. At this point a first order transition from $\psi = 0$ to $\psi \approx \pm 1.05$ takes place. Again, this is clear evidence for a first order triple point of the RW transition.

Being sure that we found a first order RW transition branching point with first order lines ("legs") departing from it, we will now depict the phase diagram in the imaginary chemical potential region. The $\theta - T$ plane is shown on the left side of Fig. 5.4. First, we find the RW transitions at $\theta/(\pi/3) = 1, 2, \ldots$ starting at $T_{RW} = 190.3$ MeV. But as a new feature this time first order lines are departing from it. In the present setup the legs end in second order endpoints at $\theta/(\pi/3) \approx 1 \pm 0.09$, $\theta/(\pi/3) \approx 2 \pm 0.09$ etc.

The deconfinement crossover transition has been defined via the inflection point of the absolute value of the modified Polyakov loop (criterion B). At vanishing chemical potential it occurs at $T \approx 175$ MeV via this criterion. The deconfinement crossover lines join into the second order endpoint of the RW legs.

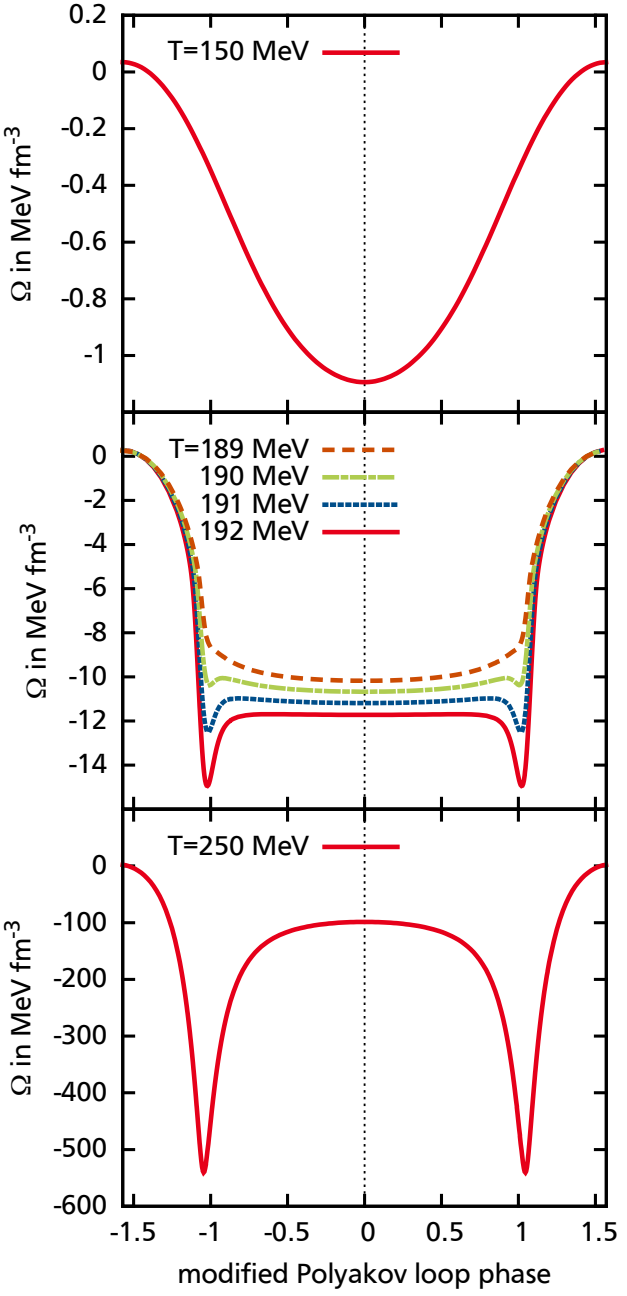

Figure 5.3: Potential surface at $\theta/(\pi/3) = 1$ for various temperatures below, around and above the RW transition endpoint at $T_{RW} = 190.3$ MeV.

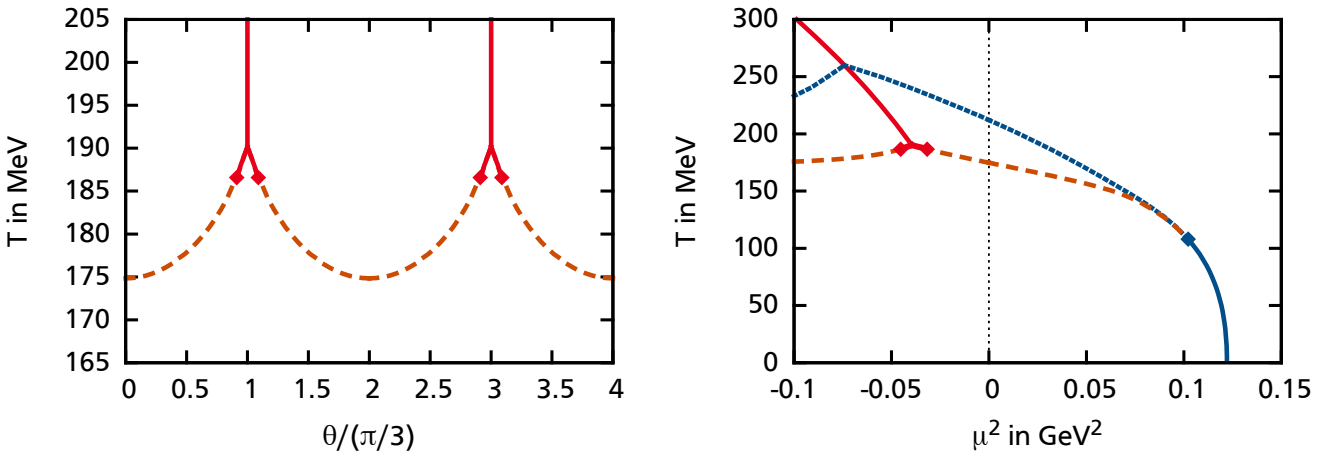

Figure 5.4: Left: Phase diagram in the $\theta - T$ plane. Solid lines denote first order RW transition ending with second order endpoint at each leg. Dashed lines denote the deconfinement crossover transition.
Right: Phase diagram in the $\mu^2 - T$ plane. In the imaginary chemical potential region solid lines denote first order RW transitions ending with a second order endpoint at each leg. In the real chemical potential region the solid line denotes a first order chiral transition ending with a second order endpoint. Dashed (dotted) lines denote the deconfinement (chiral) crossover transition.

In the $\mu^2 - T$ phase diagram on the right of Figure 5.4 we additionally show the chiral crossover transition which has been defined via the maximum of the chiral susceptibility. At vanishing chemical potential it occurs at $T \approx 212$ MeV. The second order endpoint of the first order chiral phase transition lies at ($T_{\mathrm{CEP}} = 108$ MeV, $\mu_{\mathrm{CEP}} = 320$ MeV). In the endpoint deconfinement and chiral crossover transitions join (in the case of the aforementioned crossover criteria).

In the following part we will analyze the dependence of the RW transition endpoint on certain model parameters.

First, we will check the influence of the regularization scheme. In Fig. 5.1 we see results for the order parameters using method I (only divergent vacuum integrals are cut off) and method II (vacuum and medium parts of the integrals are cut off). There is no qualitative change in the depicted quantities. Quantitatively the RW endpoint is at slightly higher temperature and the chiral crossover shifts to higher temperature if we go from method I to II.

As the next step we change the T_0 parameter of the Polyakov loop potential. T_0 denotes the critical temperature in the pure gauge limit, which means the temperature at which the potential leads to a first order deconfinement phase transition. As stated before, T_0 can change if dynamical quark degrees of freedoms are considered. In Fig. 5.5 (left pane) we show the effective quark mass as function of the temperature for different values of T_0. Lowering T_0 also lowers T_{RW} – a value of $T_0 = 190/212/270$ MeV leads to $T_{RW} \approx 172/190/238$ MeV. Also the chiral crossover is influenced by the change of T_0. For higher T_0 the chiral crossover approaches the RW transition endpoint (also in terms of T/T_{RW}). The modified Polyakov loop is almost unchanged if plotted over T/T_{RW} and is therefore not shown in the figure.

The right pane of Fig. 5.5 shows the effective mass for different values of the bare quark mass m_0. We find that T_{RW} increases slightly with m_0. Again, hardly any change is visible in Ψ as

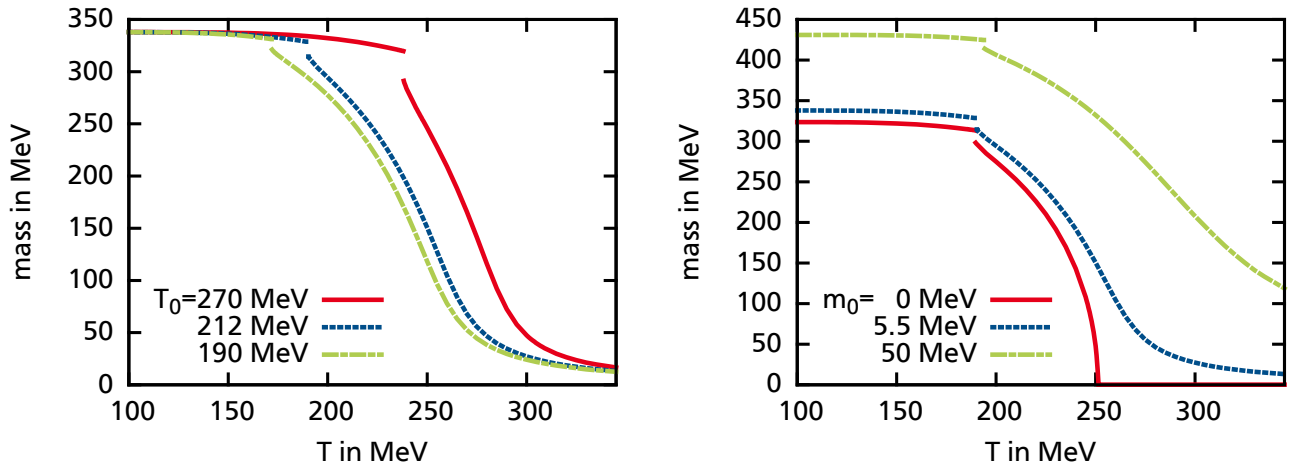

Figure 5.5: Left: Temperature dependence of quark mass for various values of the Polyakov loop potential parameter T_0 at $m_0 = 5.5$ MeV.
Right: Temperature dependence of the constituent quark mass for various values of the bare quark mass m_0 at $T_0 = 212$ MeV. All curves at $\theta = \pi/3$.

function of T/T_{RW}. We recognize that the transition is of first order for all values of m_0, from the chiral limit up to high bare quark masses.

We want to investigate the m_0-dependence in more detail as we expect that the RW transition becomes stronger for higher bare quark masses. Particularly, we will study the first order RW legs for different m_0. Results are shown in Figure 5.6: In the first half period of the $\theta - T$ phase diagram first order transition lines for several values of m_0 are presented. With increasing bare quark mass, the RW legs continue to lower θ until, at some critical value of $m_0 \approx 180$ MeV, the RW legs touch the temperature axis.

As an example we show results for $m_0 = 200$ MeV in the $\mu^2 - T$ plane, see Fig. 5.7. Indeed, the RW leg crosses the temperature axis, extends into the real chemical potential area and ends in a second order endpoint, in this specific case at about $\mu = 80$ MeV.

5.3.2 Fukushima Polyakov loop potential

In this section we will focus our analysis on the Polyakov loop potential by Fukushima which was employed in [27]. We can confirm the result that the RW transition endpoint is of second order in their setup. Parameters used were $a = 664$ MeV as usual and $b = 0.015\,\Lambda^3$ was chosen to reproduce the deconfinement crossover transition around $T_c = 180$ MeV as proposed by two-flavor lattice QCD data.

Next, we extend their studies and vary the parameter b in $\mathcal{U}_{\text{Fuku}}$, which gives the relative strength of "gluon" to quark contributions to the pressure as it is an overall factor in the Polyakov loop potential (thus increasing b means making the Polyakov loop potential more important). In the limit of large b we expect the system to approach the pure gauge case as quark contributions are suppressed, hence a first order transition at $T_c = 270$ MeV will occur along the temperature axis.

In Figure 5.8 we summarize the behavior of various transition temperatures in dependence of the parameter b. Let us first concentrate on the behavior of the RW endpoint. A larger b

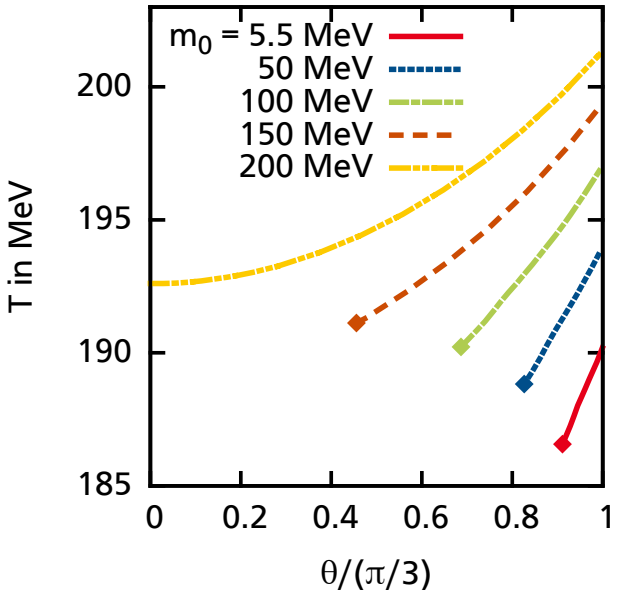

Figure 5.6: RW legs in the $\theta - T$ phase diagram for different values of the bare quark mass m_0. Each line ends in a second order endpoint. The line belonging to the highest mass extends into the real chemical potential region.

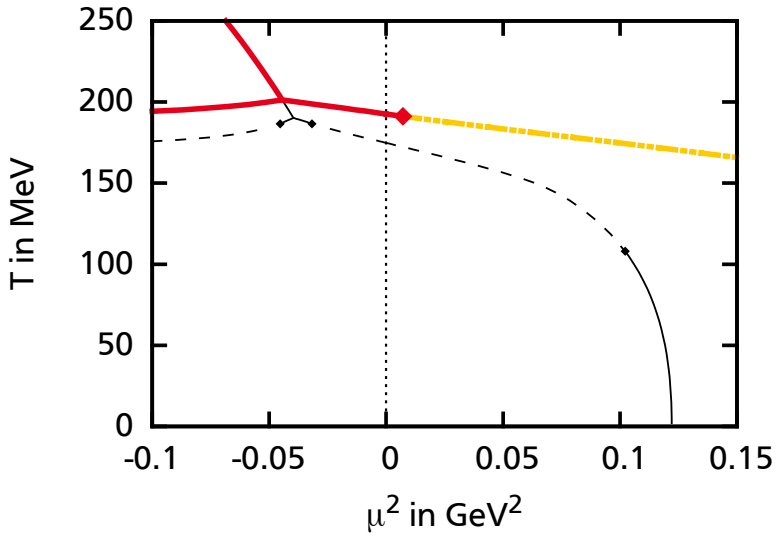

Figure 5.7: Phase diagram in $\mu^2 - T$ plane for a very high bare quark mass $m_0 = 200$ MeV. Solid (dashed) lines show first order RW (deconfinement crossover) transitions. For comparison, thin lines show respective transitions for the standard value of $m_0 = 5.5$ MeV, compare Fig. 5.4.

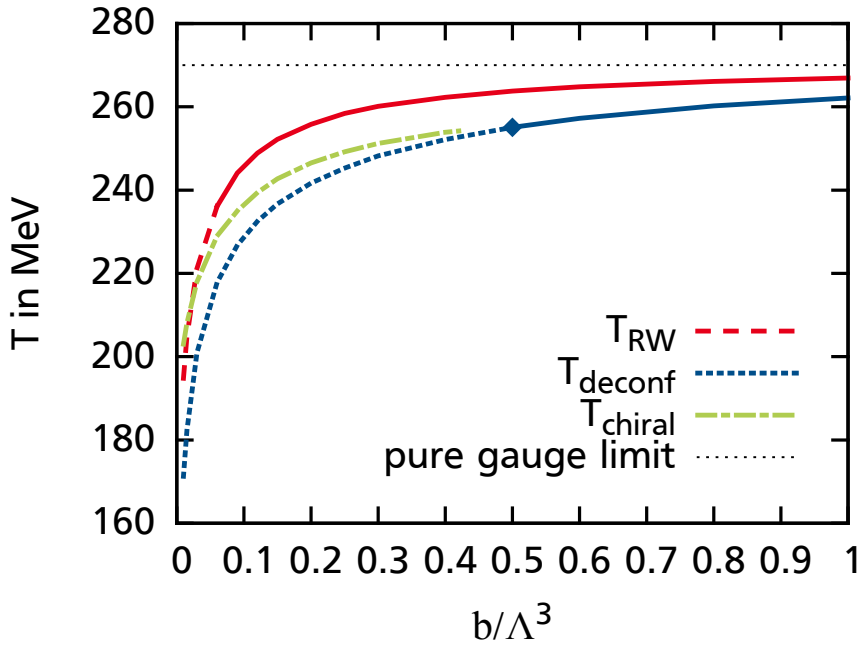

Figure 5.8: Dependence of the RW transition endpoint temperature at $\theta/(\pi/3) = 1$, the deconfinement phase transition temperature at $\theta = \mu = 0$ and the chiral phase transition temperature at $\theta = \mu = 0$. The RW transition endpoint is of second (first) order in the dashed (solid) region. Deconfinement and chiral transitions are of crossover type (of first order) in the dashed (solid) case. At the dot the deconfinement transition is of second order. See text for the crossover criteria.

parameter leads to a higher RW transition temperature. As the influence of the quark chemical potential decreases with increasing b, the RW transition temperature converges to the pure gauge limit at zero chemical potential, $T_c = 270$ MeV. The order of the RW transition endpoint changes at about $b = 0.09\,\Lambda^3$ from second order (below) to first order (above).

Furthermore the chiral and deconfinement crossover transition temperatures at $\mu = 0$ are affected by raising the b parameter as shown in the figure. Like before, we define the chiral crossover transition via the maximum of the chiral susceptibility (criterion C), and the deconfinement crossover transition via the maximal temperature derivative (criterion B). All transition temperatures approach the pure gauge limit $T_c = 270$ MeV from below. The difference between T_{chiral} and T_{deconf} becomes smaller for larger b, however T_{chiral} is always larger than T_{deconf}. Above $b = 0.42\,\Lambda^3$ the correct maximum of the chiral susceptibility cannot be determined, since the deconfinement transition mixes into the chiral susceptibility and produces a stronger maximum which even changes into a jump when the deconfinement transition becomes first order. This happens when the RW leg reaches into the real chemical potential region above $b = 0.5\,\Lambda^3$.

We additionally checked the dependence of the order of the RW endpoint on the quark mass (for $b = 0.015\,\Lambda^3$). At a bare quark mass of $m_0 > 600$ MeV the RW transition endpoint changes to first order. Since this mass is of the order of the momentum cutoff (and the dynamical mass is even higher), this kind of analysis is beyond the applicability of the present model.

5.4 Discussion

To complete the picture we want to state that the polynomial Polyakov loop potential gives similar results as the parameterization by Fukushima. The RW transition endpoint is of second order for the standard value of m_0 and becomes first order for high values of m_0. However for the polynomial potential the critical value of m_0 is even higher than for the Fukushima potential.

Summarizing, in all setups we were able to find a first order transition if either the quark mass was high enough or the relative strength of the Polyakov loop potential was increased. Both aspects were expected from the model. The transition from a second order endpoint to a first order triple point when increasing the quark mass was found in agreement with lattice QCD findings. A change to a first order transition at the endpoint for small quark masses which was seen in lattice QCD calculations could not be observed (except in the case when the transition is first order for all values of the bare quark mass). It might occur though in a very unnatural parameter region that we did not test.

The logarithmic parameterization of the Polyakov loop potential appears to have the strongest influence on the quark sector as the RW endpoint is of first order right from the start. This is in agreement with our findings in the previous chapter. We found first order lines departing from the first order endpoint. For high values of the bare quark mass they even reached into the real chemical potential region.

To go a step further, we performed first analyses in the initially described PNJL model with $2+1$ flavors. We find the same behavior for the standard values of the bare quark masses: the logarithmic potential shows a first order, polynomial and Fukushima potentials show a second order transition at the RW endpoint. It would now be interesting to calculate a "Columbia plot"-style graph where the order of the RW transition endpoint is shown in dependence of the light and strange quark masses. This is not only possible in the PNJL model but is also feasible for lattice QCD and could be a valuable test of the PNJL model.

6 Summary and outlook

We successfully implemented the PNJL model following Ref. [31] and extended it to imaginary chemical potential following Refs. [23, 24, 26, 27]. As a new feature we also included the strange quark. Phase diagrams in the real and imaginary chemical potential region have been determined and analyzed using different Polyakov loop potentials and different crossover criteria. We performed several extrapolations of crossover transition lines using polynomial ansätze from imaginary to real chemical potential. Results are partly promising but the method is not yet reliable. More sophisticated fit functions seem to be necessary in order to reproduce the correct behavior at real chemical potential.

Furthermore, in the two-flavor PNJL model we analyzed a specialty of QCD at imaginary chemical potential, which is also present in the PNJL model: the Roberge-Weiss transition and in particular its endpoint. We find that the order of the RW endpoint strongly depends on the chosen Polyakov loop potential and on its relative strength. In the case that the endpoint is first order we find first order lines departing from it, which – in certain parameter regions – can reach up to and into the real chemical potential region. Our investigation can be extended to the $N_f = 2+1$ PNJL model, where the bare quark masses of the light and strange quarks can be varied independently. The resulting dependence of the orders of the RW endpoint on the light and strange quark masses can be depicted in a "Columbia plot"-style graph which is also computable within lattice QCD.

Bibliography

[1] P. Braun-Munzinger and J. Wambach, *Rev. Mod. Phys.* **81**, 1031 (2009), arXiv:0801.4256.

[2] M. G. Alford, A. Schmitt, K. Rajagopal and T. Schäfer, *Rev. Mod. Phys.* **80**, 1455 (2008), arXiv:0709.4635.

[3] *The XXVI International Symposium on Lattice Field Theory*. **LAT2008**. Proceedings of Science (2008).

[4] Y. Aoki, Sz. Borsanyi, S. Durr, Z. Fodor, S. D. Katz, S. Krieg and K. K. Szabo, arXiv:0903.4155 (2009).

[5] F. Karsch, *Lect. Notes Phys.* **583**, 209 (2002), arXiv:hep-lat/0106019.

[6] O. Philipsen, *PoS* **LAT2005**, 016 (2006), arXiv:hep-lat/0510077.

[7] C. R. Allton, M. Döring, S. Ejiri, S.J. Hands, O. Kaczmarek, F. Karsch, E. Laermann and K. Redlich, *Phys. Rev. D* **71**, 054508 (2005), arXiv:hep-lat/0501030v2.

[8] P. de Forcrand and O. Philipsen, *Nucl. Phys. B* **642**, 290 (2002), arXiv:hep-lat/0205016.

[9] M. D'Elia and M. P. Lombardo, *Phys. Rev.* **67**, 014505 (2003), arXiv:hep-lat/0209146.

[10] L. K. Wu, X. Q. Luo and H. S. Chen, *Phys. Rev. D* **76**, 034505 (2007), arXiv:hep-lat/0611035.

[11] P. Cea, L. Cosmai, M. D'Elia, C. Manneschi and A. Papa, *Phys. Rev. D* **80**, 034501 (2009), arXiv:0905.1292.

[12] A. Roberge and N. Weiss, *Nucl. Phys. B* **275** (1986).

[13] Z. Fodor and S. D. Katz, *Phys. Lett. B* **534**, 87 (2002), arXiv:hep-lat/0104001.

[14] Y. Nambu and G. Jona-Lasinio, *Phys. Rev.* **122**, 345 (1961).

[15] Y. Nambu and G. Jona-Lasinio, *Phys. Rev.* **124**, 246 (1961).

[16] S. P. Klevansky, *Rev. Mod. Phys.* **64**, 649 (1992).

[17] M. Buballa, *Phys. Rep.* **407**, 205 (2005), arXiv:hep-ph/0402234.

[18] T. Hatsuda and T. Kunihiro, *Phys. Rep.* **247** (1994), arXiv:hep-ph/9401310.

[19] K. Fukushima, *Phys. Lett. B* **591**, 277 (2004), arXiv:hep-ph/0310121.

[20] D. Scheffler, *NJL model study of the QCD phase diagram using the Taylor series expansion technique*, BSc thesis, TU Darmstadt (2007).

[21] S. Roessner, C. Ratti and W. Weise, *Phys. Rev. D* **75**, 034007 (2007), arXiv:hep-ph/0609281.

[22] M. Wagner, *The Chiral and Deconfinement Phase Transitions in Strongly Interacting Matter*, PhD thesis, TU Darmstadt (2009), urn:nbn:de:tuda-tuprints-13174.

[23] Y. Sakai, K. Kashiwa, H. Kouno and M. Yahiro, *Phys. Rev. D* **77**, 051901 (2008), arXiv:0801.0034.

[24] Y. Sakai, K. Kashiwa, H. Kouno and M. Yahiro, *Phys. Rev. D* **78**, 036001 (2008), arXiv:0803.1902.

[25] K. Kashiwa, Y. Sakai, H. Kouno, M. Matsuzaki and M. Yahiro, *J. Phys. G: Nucl. Part. Phys.* **36**, 105001 (2009), arXiv:0804.3557.

[26] Y. Sakai, K. Kashiwa, H. Kouno, M. Matsuzaki and M. Yahiro, *Phys. Rev. D* **79**, 096001 (2009), arXiv:0902.0487.

[27] H. Kouno, Y. Sakai, K. Kashiwa and M. Yahiro, *J. Phys. G: Nucl. Part. Phys.* **36**, 115010 (2009), arXiv:0904.0925.

[28] M. D'Elia and F. Sanfilippo, *Phys. Rev. D* **80**, 111501 (2009), arXiv:0909.0254.

[29] O. Philipsen, FAIR Lattice QCD Days Nov. 2009.

[30] D. Scheffler, *The PNJL model with imaginary chemical potential*, Master project proposal, TU Darmstadt (2009).

[31] K. Fukushima, *Phys. Rev. D* **77**, 114028 (2008), arXiv:0803.3318.

[32] K. Holland and U.-J. Wiese, arXiv:hep-ph/0011193 (2000).

[33] H. Hansen, W. M. Alberico, A. Beraudo, A. Molinari, M. Nardi and C. Ratti, *Phys. Rev. D* **75**, 065004 (2007), arXiv:hep-ph/0609116.

[34] C. Ratti, M. A. Thaler and W. Weise, *Phys. Rev. D* **73**, 014019 (2006), arXiv:hep-ph/0506234.

[35] F. Karsch, *PoS* **LAT2007**, 015 (2007), arXiv:0711.0661.

[36] B.-J. Schaefer, J. M. Pawlowski and J. Wambach, *Phys. Rev. D* **76**, 074023 (2007), arXiv:0704.3234.

[37] A. Barducci, R. Casalbuoni, G. Pettini and R. Gatto, *Phys. Lett. B* **301**, 95 (1993), arXiv:hep-ph/9212276.

[38] C. Sasaki, B. Friman and K. Redlich, *Phys. Rev. D* **75**, 074013 (2007), arXiv:hep-ph/0611147v4.